UNCLASSIFIED
SECURITY CLASSIFICATION OF

AD-A144 528

(4)

ON PAGE

1a REPORT SECURITY CLASSI	RICTIVE MARKINGS
Unclassified	N/A
2a SECURITY CLASSIFICATION AUTHORITY	3. DISTRIBUTION/AVAILABILITY OF REPORT
	Approved for public release; distribution unlimited
2b DECLASSIFICATION/DOWNGRADING SCHEDULE	
4 PERFORMING ORGANIZATION REPORT NUMBER(S)	5 MONITORING ORGANIZATION REPORT NUMBER(S)
Final Report #1	AFOSR-TR- 84-0635
6a NAME OF PERFORMING ORGANIZATION: Columbia University/Osgood/ Electrical Engineering	6b OFFICE SYMBOL (If applicable): N/A
7a NAME OF MONITORING ORGANIZATION: AFOSR/NP	
6c ADDRESS (City, State and ZIP Code): 1330 Mudd, 520 W 120 Street, New York, N. Y. 10027	7b ADDRESS (City, State and ZIP Code): ~~Box 20~~ Bolling AFB, DC 20332
8a NAME OF FUNDING/SPONSORING ORGANIZATION: USAF, AFSC under Adv. Research Projts Agency (DOD)	8b OFFICE SYMBOL (If applicable):
9 PROCUREMENT INSTRUMENT IDENTIFICATION NUMBER: F49620-82-K-0008	
8c ADDRESS (City, State and ZIP Code): Air Force Office of Scientific Research, Building 410/Bolling AFB DC 20332	10 SOURCE OF FUNDING NOS

PROGRAM ELEMENT NO	PROJECT NO	TASK NO	WORK UNIT NO
61102F	2301	A1	

11 TITLE (Include Security Classification): Direct Writing of Microstructures for Microelectronics

12. PERSONAL AUTHOR(S): Richard M. Osgood, Jr.

13a TYPE OF REPORT	13b TIME COVERED	14 DATE OF REPORT (Yr., Mo., Day)	15 PAGE COUNT
Final Report	FROM 810101 TO 831231	840709	

16 SUPPLEMENTARY NOTATION

DTIC ELECTE AUG 2 0 1984

17 COSATI CODES			18 SUBJECT TERMS (Continue on reverse if necessary and identify by block number): A
FIELD	GROUP	SUB GR	Dir. Writing/Microstructures/Microelectronics

19 ABSTRACT (Continue on reverse if necessary and identify by block number):

A program to investigate direct laser writing for semiconductor processing is described. In this program the following results were obtained:

1) The first reported fabrication of submicrometer diffraction gratings in GaAs
2) Development of a new technique for writing patterns of the dielectric material SiO_2
3) Measurement of the Conductivity and properties of metal interconnects
4) The first demonstration of laser-enhanced plasma etching, and
5) The first observation of deep-UV enhanced liquid etching of GaAs and the production of 2-μm through wafer vias using this technique.

DTIC FILE COPY

20 DISTRIBUTION AVAILABILITY OF ABSTRACT	21 ABSTRACT SECURITY CLASSIFICATION
UNCLASSIFIED/UNLIMITED ☒ SAME AS RPT ☐ DTIC USERS ☐	

22a NAME OF RESPONSIBLE INDIVIDUAL	22b TELEPHONE NUMBER (Include Area Code)	22c OFFICE SYMBOL
~~Diane Dade~~ Dr Schlossberg	202) 767-~~4951~~ 4906	NP

DD FORM 1473, 83 APR EDITION OF 1 JAN 73 IS OBSOLETE

Unc

SECURITY CLASSIFICATION OF THIS PAGE

84 08 17 071

AFOSR-TR- 84-0635

Sponsored by

Advanced Research Projects Agency (DOD)

(1) ARPA Order 4487

(2) Program Code 2D10

(3) The Trustees of Columbia University in the City of New York

(4) Start Date: January 1, 1981

(5) End Date: December 31, 1983

(6) Contract Amount: $421,453.00

(7) Contract Number: F49620-82-K-0008

(8) Principal Investigator: Richard M. Osgood, Jr.
Phone Number: (212) 280-4462

(9) Program Manager: Dr. Howard Schlossberg
Phone Number: (202) 767-4906

(10) Title: Direct Writing of Microstructures for Microelectronics

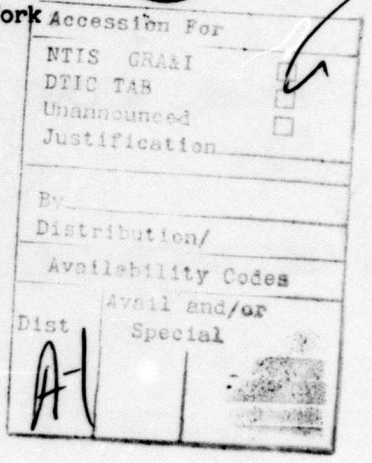

The views and conclusions contained in this document are those of the authors and should not be interpreted as necessarily representing the official policies, either expressed or implied, of the Defense Advanced Research Projects Agency or the U.S. Government.

Approved for public release;
distribution unlimited.

84 08 17 071

DIRECT WRITING OF MICROSTRUCTURES FOR MICROELECTRONICS

Department of Electrical Engineering

and

Columbia Radiation Laboratory

Columbia University

Final Technical Report

for

Defense Advanced Projects Agency

and

Air Force Office of Scientific Research

January 1, 1981 - December 31, 1983

R.M. Osgood

Principal Investigator

Table of Contents

ABSTRACT

A program to investigate direct laser writing for semiconductor processing is described. In this program the following results were obtained:

(1) The first reported fabrication of submicrometer diffraction gratings in GaAs;

(2) Development of a new technique for writing patterns of the dielectric material, SiO_2;

(3) Measurement of the conductivity and properties of metal interconnects;

(4) The first demonstration of laser-enhanced plasma etching; and

(5) The first observation of deep-UV enhanced liquid etching of GaAs and the production of 2-μm through wafer vias using this technique.

I. RESEARCH OBJECTIVES FOR DIRECT WRITING OF MICROSTRUCTURES FOR SOLID-STATE ELECTRONICS

A. Demonstration of Laser-Controlled Plasma Etching

1. Construction of Apparatus.

- o Modification of existing plasma-etch machine to allow scanning of optical beam on substrate.
- o Development of optical diagnostics for etching-rate measurement.

2. Etching on Insulating Substrates.

- o Etching of semi-insulating GaAs using cw Ar+ laser.
- o Etching of SiO_2 using cw Ar+ laser.
- o Investigate enhancement of large-area etching using very-short-wavelength F_2-excimer laser.

3. Etching of Semiconducting Surfaces.

- o Etching of doped-Si surfaces.
- o Etching of doped-GaAs surfaces.

B. Direct Writing of Si_3N_4.

1. Formation of Si_3N_4 via Laser CVD Techniques.

- o Measurement of growth rate versus laser power, gas pressure.
- o Characterize breakdown in photodeposited Si_3N_4 line.

2. Formation of Si_3N_4 via direct uv photochemistry.

- o Perform measurements listed above.

C. Applications in Device Fabrication

1. Through-wafer-via Formation in GaAs

- o Continue characterization of the existing etching process.
- o Increase the etching rate in thick wafers and control the dark etching rate.
- o Develop rapid gas-phase etching for GaAs, as a possible alternate etching technique.
- o Develop metallization technique for filling vias with conductive materials.
- o Demonstrate via formation for a working microwave FET.

2. Antennae Writing for Submillimeter Devices

- o Set up direct-writing metallization apparatus.
- o Characterize and optimize conductivity of metal lines.
- o Set up submillimeter receiver system with Schottky-barrier detector.
- o Observe detected signal while simple dipole antenna pattern is written.

II. DEMONSTRATION OF LASER CONTROLLED PLASMA ETCHING

There are several reasons why it may be desirable to enhance the rate of a plasma etching process with a laser beam. First, in many soft, semiconducting materials such as GaAs, it is important to achieve maximum etch rate with minimal ion bombardment, since surface damage often accompanies the latter. One of the reasons that ion bombardment seems an unavoidable aspect of plasma or ion assisted etching is that physical action is often necessary to remove adlayers of reaction products or other chamber contaminants. However, a number of recent experiments in this and other laboratories have shown that low levels of laser light can remove these layers, although the exact mechanism for this removal seems unclear at present. Thus by subjecting the surface to illumination in a plasma etching reaction it may be possible to operate the reactor in a region where physical bombardment and its concomitant surface damage is not necessary for satisfactory high etch rates.

Second, for a variety of reasons, including surface cleanliness and the ability to generate highly reactive species, plasma etching is an important fabrication tool in modern microelectronics. One desirable capability, however, is absent from plasma processing - namely the ability to do local processing; in other words if a particular fabrication step should require that the etching be confined or enhanced in one region of a semiconductor chip this can not be done at present in commercial reactors without separatey masking the other region of the chip. If the region of local etching is small compared to the remainder of the I.C. real estate, the additional masking step, of course, subjects a major portion of the wafer to the several additional

processing steps thereby defeating at least a portion of the original reason for using dry etching. By using a maskless technique for enhancing plasma etching, which is based on pattern or focussed laser light, local plasma processing can be done without requiring additional surface processing of the wafer.

In the set of experiments described here, we used visible laser light to influence the etching of Si wafers in a commercial planar plasma etching system. A CF_4/O_2 plasma, at, typically, 100 torr gas pressure was used. By modifying the r.f. electrode through the installation of a laser port, we were able to focus the laser onto the Si surface with an imaging system external to the etching apparatus.

The effect of the laser beam on the etch rate of p-type Si was investigated by varying the laser power density from 150 mW/cm^2 to 4 kW/cm^2. For each measurement made, the dark etch rate and the photon-enhanced etch rates are compared. The resulting data showing the Si etch rate in the focal spot are plotted in Fig. 2 of Appendix A.

The graph shows that the etch rate is light-enhanced even at low laser power density (150 mW/cm^2). This enhancement increases with laser power density and reaches 50% of the dark etch rate at the maximum laser power we used. The dark etch rate remained constant at 0.2 $\mu m/min$ throughout the experiment. Although we did not explicitly examine the resolution of the photon-induced process, it appears to be quite high. For example, an interference pattern of the laser beam resulted in etch features as small as 10 μm.

Note that in a previous, separate set of experiments performed using the same apparatus, we had shown that the etch rate is

significantly increased when the Si wafer is heated in bulk by the laser beam. However, at the lower laser power densities, the enhancement appears to result from a nonthermal process, since heating is negligible in this region. In order to investigate whether this process is dependent upon electron/hole pair creation, n-type Si of the same conductivity as the p-type Si (1-2 Ω-cm) was investigated. We found no difference in the photon-induced etch enhancement. It should be noted, however, that even at low laser power density a considerable number of photogenerated carriers are present, perhaps eliminating any difference in their effect on the etch rate of p and n-type Si.

In conclusion, we have demonstrated that significant photon-induced etch rates are possible when a laser beam illuminates the surface of an Si wafer in a plasma etcher. The effect of low laser power densities is a nonthermal one. Using a focused laser the light enhancement can be employed to achieve maskless definition of the etching pattern. Considerable additional detail can be found in the paper preprint of Appendix A.

III. DIRECT WRITING OF INSULATORS

A. Direct Deposition of SiO_2 Using Excimer Laser Irradiation

We chose to produce oxide layers on single crystalline silicon using a spin-on silicate with subsequent laser irradiation. This material is easily applied. Studies using it have a value beyond the formation of simple oxide layers since silicates and related compounds form the basic chemical of spin-on inks and dopants which are used commonly in the microelectronics industry in intimate contact with the Si wafer. Low-temperature oxides have been produced over a 1-cm area

using only two laser pulses. These oxide layers are smooth and of uniform thickness.

B. Direct Writing Instrumentation

The Instrumentation for direct writing was received during this period; it includes a 15-W, visible-wavelength laser, a Zeiss ultraviolet microscope with fast scanning stage, and an HP-87 computer. The funds to purchase this equipment were provided from JSEP through the Columbia Radiation Laboratory.

A software system was written which interfaces the HP-87 minicomputer with an Aerotech Microdex x-y translation stage and the Zeiss Universal microscope with fast scanning stage.

The system allows:

1. Varying feed rate control for each line written
2. Generation of an array of differing patterns
3. Simplified editing
4. Incorporation of an integrated shutter system operating on positive or negative logic in addition to the manual control.
5. Specification of the pattern in terms of coordinates
6. Printer/plotter interfacing allowing simultaneous video monitoring of patterns

The system is fully interactive and provides scaling of the patterns down to the resolution of the stages drives: 0.25 μm for the Microdex and 0.5 μm for the Zeiss. In addition, we tested and built a digital circuit for smooth ramping and lowering of the laser power. This will enable us, for example, to write a uniformly varying metal conductor on a silicon surface.

Finally, because of the mutual reactivities of the metallorganic

gas used in the metal writing (below), it was necessary to design two dedicated high vacuum systems for handling these gases. During this contract, we designed and fabricated two separate gas-handling systems.

C. Direct Writing of SiO_2

In the second maskless technique for patterning silicon dioxide layers from a spin-on organosilicates, a focused laser beam is used to directly write silicon dioxide patterns on a variety of substrates. The quality of the oxide layers is at least as good as that obtained in thermally cured spin-on glass. An added advantage of this technique is the ability to readily vary the thickness of the oxide layer as a function of the exposure time. Some possible applications include local masking for GaAs, SiO_2 waveguides for silicon wafers and new device structures requiring a variable oxide thickness.

The writing of oxide layers is accomplished by using an argon ion laser tuned to 514.5 nm. A microscope objective (20X, N.A. = 0.35) coupled with a Michelson interferometer is used to focus the laser beam onto the sample. The sample is mounted on a vacuum chuck which is attached to a computer-controlled, X-Y translation stage. The stage is driven by a stepper motor with 0.4 μm resolution and linear scanning rates from 4 μm/sec to 200 μm/sec. Blanking of the laser beam is accomplished with a computer-controlled mechanical shutter. The starting material, an experimental material provided by Allied Corporation known as X-200A, is an organosilicate material in an organic based solvent.

Curing of organosilicate films by laser-induced heating is significantly different from conventional thermal curing in a furnace. Furnace curing requires that either the temperature be slowly ramped or

a low-temperature cure (100° C) precedes the final high temperature cure. Curing of the organosilicate occurs from the outer surfaces of the film toward the center. As the organosilicate cures in the furnace, the volatile components must pass through the cured outer regions. If the sample temperature is not ramped in the furnace or preceeded by a low temperature cure, surface cracks resulting from the escaping voltile components can result. In laser curing, on the other hand, since the organosilicate is essentially transparent in the visible region, the laser beam passes through the film and strikes the surface of the silicon substrate where it is partially absorbed thereby heating it up. Curing of the organosilicate film occurs from the organosilicate-substrate interface outward allowing volatile components to escape easily, since the surface of the layer had not been cured first. This allows for high substrate surface temperatures during curing without cracking the organosilicate layer.

Writing was attempted over a wide range of scan speeds, focal-spot sizes and laser powers. Typical conditions were 250 mW in a 3 μm-diameter spot which corresponds to 4 MW/cm^2 and a sample translation speed of 100 μm/sec. With theses experimental perameters, a smooth, continuous line could be obtained. To remove the unexposed material, it is necessary to rinse the wafer with methanol. The cured pattern then remains. In order to obtain a complete removal of the unexposed material, it is necessary to carefully preclean the wafers and to keep the samples under conditions of low relative humidity.

A further result of the organosilicate curing from the organosilicate-substrate interface outward is that if the exposure time

is insufficient to cure the entire thickness of the deposited organosilicate, a cured organosilicate layer thinner than the deposited layer can be obtained. This gives a thickness, or z-axis control over the oxide layer. This smooth control over the thickness of local regions of oxide is not easily achieved through conventional photolithography. In addition to the thickness variation, the width of the oxide lines is also a function of the translation speed and incident power.

Electron micrographs of the laser cured SiO_2 lines are shown in the illustration of Appendix B. This Appendix also gives more detail on the adlayer conditions.

We have experimented with substrate materials other than silicon. These include the compound semiconductors CdS and GaAs and the dielectric SiO_2. In each case, after a proper surface preparation and adjustment of incident laser power to account for different absorption and thermal properties, direct writing of oxide lines was readily accomplished. In particular for GaAs, surface preparation consisted of a standard degreasing and oxide removing cleaning procedure. Consistent with the thermal and absorption properties of GaAs, direct writing was done at 100 mW for scan speeds similar to those used above.

In conclusion, we have demonstrated a method of patterning silicon dioxide layers on various substrate materials without the use of a mask. The technique relies upon the curing of a spin-on organosilicate by localized heating with a focused laser beam. Translation of the sample provides for maskless pattern generation. Line widths as low a 1 μm have been obtained (See Appendix B). Both line width and line thickness are affected by the sample translation speed and the incident laser

power. This means that silicon dioxide lines of continuously varying thickness can be written on the wafer surface.

IV. APPLICATIONS IN DEVICE FABRICATION

A. Through-wafer via Formation in GaAs

Controlled etching of compound semiconductors is an important processing step for the fabrication of electronic devices, e.g. integrated optical components and fast microwave devices. Previously, we reported that light-enhanced, electrodless, wet etching can be successfully used for maskless patterning of compound semiconductors. The etching is influenced by the number of carriers present at the semiconductor surface, and thus allows a light pattern to be engraved in the semiconductor surface In this report, we describe two experiments at different wavelengths in which we continue to utilize the light-enhanced, wet etching of single-crystalline GaAs. First, we investigated the application of visible laser light to the drilling of via holes in GaAs. Second, for the first time the effects and the utility of deep-ultraviolet (UV) light (257 nm) in maskless via hole wet etching were explored.

In initial experiments on producing via hole structures in GaAs a focused visible Ar^+ ion laser was employed. Limited success was reached with only small aspect ratio via holes being produced. The drawbacks which limit using visible laser light for this application include the large absorption depth in GaAs, and the laterial spreading of photogenerated carriers in the GaAs substrate at visible wavelengths. These drawbacks are overcome by using deep-UV laser light since the absorption depth in GaAs is, typically, an order of magnitude smaller

than for visible light. In addition, creating the carriers in the band-bending region by deep UV-light reduces the lateral spreading of photogenerated carriers, and thus, higher-resolution etching is more readily obtained. Ultraviolet light can also photochemically activate the liquid or the adlayer at the solid surface and high-energy, UV photons can produce hot carriers at the semiconductor surface. Both effects may substantially change reaction rates and reaction chemistry.

The deep-UV light source, a frequency-doubled, Ar-ion laser (257 nm) was used to illuminate the semiconductor. The incident laser power density ranged from 10 mW/cm^2 to 2 kW/cm^2. The estimated temperature rise at the semiconductor surface was below 2^o C, even at laser intensities of 2 kW/cm^2; as a result, thermal effects were not important in these experiments. Generally, UV light was coupled in an optical microscope and focused with a 10X UV objective (N.A. = 0.2) on the sample, mounted inside a quartz cell filled with the etching solution. The light path through the liquid was 400 μm. The etching process was monitored with a vidicon camera, using weak, white-light illumination. In order to determine the quality and the depth of etched structures, the semiconductor was cleaved precisely across the etched structures. Typically, the cleaved surface was investigated with an optical microscope or, in some cases, with a scanning-electron-microscope (SEM).

In this report, we will discuss results on n-type, (100) GaAs (Si-doped, n-10^{18} cm^{-3}) and H_2SO_4 : H_2O_2 : H_2O solutions. Of practical importance is the fact that the dilute - H_2O_2-content solutions have an extremely small dark etching rate, but still substantial UV-enhanced etching rates. In most of our experiments, we used an 1:1:100 solution, which had a dark etching rate of less than 40 nm per minute.

Rapid and well-resolved etching in the dilute solution and at low UV-laser intensity produced high-quality via-holes in GaAs with large aspect ratios which are important for fast microwave devices. These structures were examined in a series of experiments in which the laser light was focused to a 5- 10 μm spot on the GaAs surface. By monitoring the via-hole formation and examining the cleaved cross sections afterwards, it was found that the etching slowed down as the hole depth increased. This effect may limit the wafer thickness which can be etched. For high laser intensity, the etching process begins rapidly but stops after ~80μm. For lower intensities, the hole-etching rate is slower, but more penetrating, resulting in deep, high-quality, via-holes, see Fig. 5 in Appendix C. The entrance and the exit of the etched via-holes are well defined and the surrounding area is undamaged. Another remarkable feature of these via-holes, is their vertical walls, which can be attributed to "waveguiding" of the etching beam. At the higher intensities (2 kW/cm^2), scattered and reflected light inside the hole destroys this vertical wall, and prevents further penetration. At 100 mW/cm^2, we were able to etch a 1 μm-diameter hole through a 100-μm-thick GaAs sample; at somewhat higher powers we were able to bore through a standard 250 μm wafer, although larger diameters resulted.

B. Metallization for Interconnects and On-Wafer Antennae for Submillimeter Devices

One of the major goals of this contract is to be able to achieve enough control of the photodepositon process that practical, direct-write applications can be demonstrated. Although many of the applications of direct writing require the writing of good quality conductors, there have been no previous studies of the effect of the

deposition conditions on the electrical properties of photodeposited metal lines. Also we have begun an investigation of the variations in the resistivity and microstructure of photodeposited metal conductors with changes in several deposition parameters.

Initially, our experiments on metal line writing have centered on the measurement of writing rates for conditions of varying laser power, gas pressure, and laser intensity. In addition we have examined metal writing on a variety of novel substrates including plastics and silicon dioxide structures.

In order to measure the deposition rate we used the optical attenuation of the laser beam. Absolute calibration was obtained by measuring the thickness of several of the deposits with scanning electron microscopy. The spot size of the laser used in the experiment was 3 μm.

The deposition rates which we obtained are sufficiently rapid to permit writing over small areas on integrated circuits and IC components. Before a large-area region can be written, as would be required, for example, for writing the metallization pattern on an entire wafer, much faster rates would be needed. In fact a considerable increase in writing rates over those obtained can be anticipated if both the laser intensity and pressure are increased and the existing scaling laws continue to hold. The UV laser power was increased by using a mode-locked laser, since in this case the same average power was obtained at 514.5 nm but the visible output appeared as a series of narrow, high intensity pulses. These pulses could then be more efficiently converted to the UV using nonlinear, frequency doubling.

In addition to measuring deposition rates we also examined direct-

deposition on organic substrates, including Mylar and Plexiglas. Deposition of metal on such fragile, low melting point substrates is an important capability for such applications as information storage and electric components containing polymers. Normal deposition methods are of limited use either because of substrate damage or lack of adherence. Our experiments have show, in fact, that photodeposition can be used to deposit adherent metallic lines on various polymer substrates.

Another focus of our experiments was to determine if it is possible to write complex patterns. For example, our understanding of the process physics might suggest that while writing a large pattern that metal vapor would tend to migrate to an earlier written pattern. This, in turn, would cause the pattern to fade as the writing continued. A directly written grid pattern showed that this is not the case; the lines are of uniform thickness and definition across the photograph. Writing of even more complex patterns, such as a Columbia logo showed similar constant deposition. Finally, in so far as the writing of more complex device-structures are concerned, it is of interest to show that combination of writing techniques can be used together. This ability was demonstrated by writing metal conductors over directly written SiO_2 patterns on a silicon wafer. Clearly such a structure is important in writing MOS structures.

Our experiments with electrical characterization were done with cadmium deposited onto a glass plate from dimethyl cadmium (DMCd), using the ultraviolet light from a frequency-doubled Ar+ laser. The plate contained a vacuum evaporated pattern of gold dots and was mounted in a nonflowing-gas cell. The cell was moved with a constant velocity perpendicular to the UV-beam to obtain the written features. The length,

width and thickness of the lines were determined by microscopy and surface probing. These measurements have enabled us to determine the specific resistivity of the lines and to compare these values with those of the bulk metal. The results for different DMCd pressures with and without buffer-gas are shown in Fig. 1a of Appendix D; improved values can be expected as a result of further optimization of the many possible deposition parameters. The best relative resistivity was ~4 times higher than that of bulk cadmium. In addition, in Fig. 1b of Appendix D, the variation of the resistance with respect to temperature is shown.

In photodeposition, the material growth is dominated either by the decomposition of the adlayer, on the surface, or the molecules in the gas-phase. The structural behavior of the deposited metal which influences the electrical properties is strongly dependent on the growth mechanism. the structures grown preponderantly from the adlayer exhibit light-induced surface ripples; these features cause an increase in resistivity on the low-pressure side of the deposition region. At high DMCd pressure, the growth occurs from a dense metal vapor which causes a coarse-grained nonlocal deposit with increased resistivity. At low temperature, where the adlayer growth dominates, we believe the increased resistivity is due to incomplete adlayer decomposition.

C. Optical Diffraction Gratings for Electrooptical Devices

In most of the laser chemical processing described recently the temporal coherence of the laser source has not played an important role in the processing results or physics. We have now demonstrated a laser chemical processing technique which requires that the light source have a high degree of temporal coherence, namely, laser holographic

processing. In this processing, two laser beams are interferred to produce a coherent pattern across a substrate surface. The laser light then by either a linear or nonlinear optical process, drives a chemical reaction which causes the necessary local surface alteration. Gratings are an important surface structure for integrated and discrete semiconductor optical devices. For example, because of the high dielectric constant in compound semiconductors, the spatial periodicity of the gratings must be much smaller than the free-space wavelenth used in the optical device. This high spatial resolution plus the requirement for grating profile control makes fabrication by conventional techniques difficult. We note that fabrication of gratings has historically been a standard microstructure for demonstrating and improving the process resolution. In addition, the temporal coherence of the laser source is important for recording optical information, viz for producing holograms.

1. Liquid-phase etching of GaAs

The apparatus for this experiment has been described in detail in Appendix E. Basically, a laser beam from a moderate-power, argon-ion laser passes through a spatial filter and a collimator before being split and mixed inside an optical cell containing an H_2O_2 : H_2SO_4 : H_2O etching solution. The dissolution of GaAs in this solution is influenced by the number of carriers present at the semiconductor surface. For n-type GaAs, photogenerated holes accelerate the etching rate, thus forming a photoengraved pattern in the solid surface. Although we have formed high resolution gratings on other III-V as well as on II-VI compound semiconductors, we will limit our discussion here to n-type GaAs doped with Si, $n = 10^{18}$ cm^{-3}, and with (100) crystal orientation.

Using the above experimental arrangement, we have produced 130-nm to 200-nm gratings with maximum depth-to-spacing ratios, d/s, of typically 0.2. For gratings with spacings >1 μm, the depth-to-spacing ratio exceeds 0.4, for example, 2-μm gratings had a ratio of 0.8. The gratings were uniform and without secondary ripples over a relatively large area of ~1 cm^2. This area was limited by the uniformity of the laser beam. The maximum resolution reported here was limited by the wavelength of the laser light. Recently we have used UV radiation to obtain 100-nm period gratings.

The profile of the grating grooves depends on the details of the carrier movement within the semiconductor, the relative magnitude of the dark versus light-enhanced etching rate, and the anisotropy in the etching process. We investigated the profiles of gratings on n-type GaAs for several different crystal orientations using different spacings and etching solutions. For the dilute 1:1:100 solution used in most of our experiments, we found that crystal orientation did not influence the grating profiles and etch rates. Generally, gratings with spacings >1 μm had a sinusoidal profile which is to be expected for a linear dependency between etching rate and light distribution on the surface. On the other hand, submicrometer gratings showed a deviation from a simple sinusoidal profile; typically a cusped profile was observed. This deviation cannot be explained by a simple theory based on an isotropic diffusion of the holes at the semiconductor surface. Local variations in the hole drift due to photoinduced electric fields, both normal and to the surface transverse to the surface and the interference pattern, give rise to higher-order components in the groove profile.

In general, the etching rate for the submicrometer was found to be

dependent on the grating spacing. The data was obtained by SEM photographs of the GaAs samples cleaved perpendicular to the grooves, however, in situ monitoring, using a He:Ne laser probe, yielded similar data. The slopes of the curves indicate the grating growth rate. In the first 3 to 5 minutes, the gratings grow with a constant rate. For smaller-spacing gratings, i.e. 1 μm, the rate decreases due to the lateral carrier diffusion on the surface.

By comparing the measured rates for the different spacings, an approximate diffusion length of 0.12 μm can be obtained. This diffusion length is considerably smaller than the literature value of 1 μm for the GaAs used in our experiment. We believe that this difference can be explained by the strong built-in electric field in the depletion region normal to the interface and the short carrier lifetime at the surface, due to the chemical reaction.

2. Photodeposition of Metal Grating

The experiments to investigate photodeposition of metal gratings were accomplished with a 3 - 5 mW, frequency-doubled, argon-ion laser. This laser has sufficiently short wavelength to photodissociate the metal-alkyl carrier gas, (dimethyl cadmium) used here, and, further, it has an useful temporal coherence length $\sim$20 cm. The laser beam was split and mixed on the rear surface of a quartz flat mounted on a sample-cell containing dimethylcadmium gas. The angle between the two laser beams could be adjusted so as to examine different grating spacings.

Before describing the results obtained here, we point out that high-resolution interference effects have been observed previously for photodeposition. In these cases, it was found that fringes with periods

of ~0.17 μm could be obtained in photodeposited metal. The origin of these structures has been tied to the stimulated growth of surface plasma waves in a deposit growing from photodeposited parent molecular overlayers. The fringes result from the interference of the surface waves with the incident light. While these fringes are of great scientific interest, their limited coherence length, ≥ 2 μm, makes their practical use limited.

With our experimental setup, we readily obtained submicrometer diffraction gratings as small as 300 μm. In general, the best results were obtained when the sample cell, which contained 10 torr of DMCd and 80 torr of buffer gas, was cooled to 15° C. At these temperatures physisorbed molecular layers are thick and the contribution from gas-phase photodissociation is minimized.

Grating formation by photodeposition allows direct optical monitoring of the deposition by a noninvasive optical probe; in our case an He:Ne laser was used. The probe is used by observing the minus-first-order diffracted light from the metal grating. For small modulation depths the intensity of the diffracted light is proportional to h, to the amplitude of the grating ripple. Thus the grating growth rate can be monitored through the rate of increase in the diffracted intensity.

These measurements have shown clearly one of the most striking phenomena associated with optical growth of diffraction gratings. As the angle of interference is varied sharp resonances are observed in the grating growth rates. These resonances are the result of enhanced coupling of light into surface confined waves within the metal film. The resonances occur when the grating spacing, d, is equal to an

odd multiple of half wavelengths of the surface wave which exists at the frequency of the incident optical electric filed.

At the spacing of each resonance the angle one of the diffracted orders is such that the wavevector of the light is just parallel or along the surface of the metal. Thus, each resonance represents a spacing such that the amplitude of the surface plasma wave intensity is maximized. Since the local electric field, including incident and scattered waves, determines the rate of grating growth, the deposition is fastest at resonance spacings. The grating growth rate can be increased by as much as a factor of 8 at resonance compared to that for off resonance. For the laser powers and grating areas considered here, this means that relatively dense metallic gratings can easily be grown at resonance, spacings whereas only very thin structures can be obtained at intermediate values. Appendix E gives additional details on the grating growth mechanism.

Professional Personnel

Associated with the Research Effort

Prof. Richard M. Osgood	Faculty, Principal Investigator
Prof. Edward Yang	Faculty
Dr. Heinz Gilgen	Research Scientist
Dr. Grace Reksten	Research Scientist
David Rivera	Senior Technical Assistant
Robert Krchnavek	Graduate Reseacher
Dragan Podlesnik	Graduate Researcher
William Holber	Graduate Researcher

PAPERS IN THE AREA OF LASER DIRECT WRITING SUBMITTED FOR PUBLICATION
(Papers denoted by an (*) received partial or full support from this contract)

1. R.M. Osgood, D.J. Ehrlich, T.F. Deutsch, D.J. Silversmith, and A. Sanchez, "Direct-Write Laser Fabrication: Customization, Correction, and Repair." To be published in Microelectronics - Structures and Complexity. (*)

2. A.M. Hawryluk, H.I. Smith, R.M. Osgood, and D.J. Ehrlich, "Deep UV Spatial Period Division Using Excimer Laser Sources," Opt. Lett., 7, 402 (1983).

3. C.J. Chen and R.M. Osgood, "Ultraviolet Absorption Spectra of Physisorbed Molecules," Chem. Phys. Lett., 98, 363 (1983).

4. D.V. Podlesnik, H.H. Gilgen, R.M. Osgood, A. Sanchez, and V. Daneu, "High Resolution Etching of GaAs and CdS Crystals," in Laser Diagnostics and Photochemical Processing for Semiconductor Devices, edited by R.M. Osgood, S.R.J. Brueck, and H.R. Schlossberg (North-Holland, Amsterdam, 1983). (*)

5. C.J. Chen and R.M.Osgood, "Spectroscopy and Photoreactions of Organometallic Molecules on Surfaces," in Laser Diagnostics and Photochemical Processing of Semiconductor Devices, edited by R.M. Osgood, S.R.J. Brueck, and H. Schlossberg (North-Holland, Amsterdam, 1983)

6. R.M. Osgood, S.R.J. Brueck, and H. Schlossberg, "Laser Diagnostics and Photochemical Processing for Semiconductor Devices," in Laser Diagnostics and Photochemical Processing for Semiconductor Devices, edited by R.M. Osgood, S.R.J. Brueck, and H. Schlossberg (North-Holland, Amsterdam, 1983).

7. C.J. Chen and R.M. Osgood, "Direct Observation of the Local-Field-Enhanced Surface Photochemical Reactions," Phys. Rev. Letts., 50, 1705 (1983).

8. E. Poon, E.S. Yang, H.L. Evans, W. Hwang, R.M. Osgood, "Determination of Grain Boundary Barrier Height and Interface States by a Focused Laser Beam," Appl. Phys. Lett. 42, 285 (1983).

9. C.J. Chen and R.M. Osgood, "Surface-Catalyzed Photochemical Reactions of Physisorbed Molecules," Appl. Phys., 31, 171 (1983).

10. R.M. Osgood, "Excimer Laser Interface Chemistry for Microelectronic Processing," in Excimer Lasers, Edited by C.K. Rhodes, H. Egger, and H. Pummer, (AIP New York, 1984) (to be published)

11. V. Daneu, D.J. Ehrlich, R.M. Osgood, A. Sanchez, "Reflectometric Spectroscopy of Adsorbed Molecular Layers," Opt. Lett., 8, 151 (1983).

12. D.V. Podlesnik, H.H. Gilgen, R.M. Osgood, "Direct Chemical Etching of Submicrometer Gratings in Single-Crystalline GaAs," Appl. Phys. Lett., 43, 1083 (1983).

13. C.J. Chen and R.M. Osgood, "A Spectroscopic Study of the Excited States of Dimethylzinc, Dimethylcadmium, and Dimethylmercury," J. Chem. Phys. 81, (1984) (To be published)

14. R.M. Osgood, "Laser Microchemistry and its Application to Electron Device Fabrication," Am. Rev. Phys. Chem. 34, 77 (1983). (*)

15. C.J. Chen and R.M. Osgood, "An Analytic Theory of Photodissociation of Linear Symmetric Polyatomic Molecules," J. Chem. Phys. (To be published).

16. R.R. Krchnavek, H.H. Gilgen, and R.M. Osgood, Jr.,"Maskless Laser Writing of Silicon Dioxide," J. Vac. Sci. Tech., Part B. (To be published). (*)

17. D.V. Podlesnik, H.H. Gilgen, R.M. Osgood, "Deept-UV, Light-Assisted, Wet Etching of Compound Semiconductors," in Laser-Controlled Chemical Processing of Surface, edited by A.W. Johnson and D.J. Ehrlich, 1984. (*)

18. H.H. Gilgen, D.V. Podlesnik, C.J. Chen, and R.M. Osgood, "Direct Holographic Processing Using Laser Chemistry," in Laser-Controlled Chemical Processing of Surfaces, edited by A.W. Johnson and D.J. Ehrlich, (North-Holland, Amsterdam, 1984). (*)

19. P. Brewer, S. Halle, and R.M. Osgood, Jr., "Photon-Assisted Dry Etching of GaAs, Appl. Phys. Lett. (To be published)

20. D.V. Podlesnik, H.H. Gilgen, and R.M. Osgood, Jr., "Deep-Ultraviolet Induced Wet Etching of GaAs," Appl. Phys. Lett. (submitted) (*)

21. R.M. Osgood, Jr., D.J. Ehrlich, T.F. Deutsch, D.J. Silversmith, A. Sanchez, "Laser Microchemistry for Direct Writing of Microstructures," SPIE Vol. 385 - Laser Processing of Semiconductor Devices, 1984. (*)

22. P. Brewer, S. Halle, and R.M. Osgood, Jr., "Excimer-Laser-Initiated, Dry Etching of Single Crystal GaAs," Material Research Society Symposium Proceedings, 1984.

23. D.J. Ehrlich, T.F. Deutsch, R.M. Osgood, Jr., and D.J. Silversmith, "Laser Photochemical Processing for Microelectronics," Proceedings of the 14th International Conference on Solid State Devices, March 1983, Japanese J. of Applied Physics, 22, 161 (1983). (*)

24. D.V. Podlesnik, H.H. Gilgen, R.M. Osgood, A. Sanchez, "Maskless Chemical Etching of Submicrometer Gratings in Single-Crystalline GaAs," Appl. Phys. Lett. 43, 1083. (*)

25. R.M. Osgood, Jr., "Material Deposition and Removal Using Laser-Initiated Chemistry," Journal de Physique, p. C5-133, 1983. (*)

26. C.J. Chen, H.H. Gilgen, and R.M. Osgood, Jr., "Microstructure of Photodeposited Thin Films," Microscope Semiconductor Material Conference, Oxford, 21-23, 1983.

27. P.Brewer, W. Holber, G. Reksten, and R.M. Osgood, Jr., "Laser-assisted Dry Etching of Semiconducting Materials," SPIE - Laser Processing of Semiconductor Devices, 1983. (*)

Presentations to Industry and Professional Organizations

IBM - T.J. Watson Research Center (New York)	January 1982
NATO Research Institute on Microelectronics	March 1982
CLEO 82 - Chaired Subcommittee on Laser Applications for Microelectronics Delivered Plenary Address Tuscon, AR	May 1982
Bell Telephone Laboratory (Holmdel)	May 1982
Bell Telephone Laboratory (Murray Hill)	June 1982
MIT Symposium on Surface Science (Cambridge)	June 1982
Columbia-T.J. Watson Lab Joint Seminar (New York)	July 1982
Annual American Chemical Society (Kansas City, Mo) - 1 invited talk, 1 contributed talk	September 1982
Materials Research Society (Boston, MA) 1 invited paper, 1 contributed paper. New Symposium of Laser Diagnostics and Photochemical Processing for Microelectronic Devices Organized by R.M. Osgood and S.R.J. Brueck	November 1982
Industry-Columbia Symposium on Microelectronics and Fabrication (New York)	November 1982
IBM East Fishkill Facility (East Fishkill)	November 1982
Stanford Symposium of Irradiation of Thin Films	December 1982
Excimer Laser Conf. (Incline Village)	January 1982
NATO Workshop on Industrial Applications of Laser Processing (Mons)	February 1982
Allied Corporation Seminar	February 1982
Conference on Microscopy of Semiconducting Compounds (Oxford)	March 1983

CLEO '82 - 1 invited talk, 1 contributed talk (Baltimore, MD)	May 1983
IBM T.J. Watson Lab (Yorktown Heights, N. Y.)	May 1983
MRS Europe (Strassbourg)	May 1983
N. Y. Regional A.V.S. Meeting, Rochester)	June 1983
N.E. Regional American Chem. Society Meeting	June 1983
Riken Symposium. High Efficiency Gas Lasers, Tokyo, Japan	June 1983
American Vacuum Society, Boston 1 invited paper, 1 contributed paper	November 1983
Materials Research Symposium, 1 invited talk, 3 contributed talks (Boston)	November 1983
Stanford Industrial Program of Irradiated Thin Film Technology (Stanford, CA)	December 1983
University of Berne, (Berne)	December 1983

APPENDICES

A. W. Holber, G. Reksten, and R.M. Osgood, Jr., "Laser-Enhanced Plasma Etching of Si," submitted to Appl. Phys. Lett.

B. R.R. Krchnavek, H.H. Gilgen, and R.M. Osgood, Jr., "Maskless Laser Writing of Silicon Dioxide," to be published in J. Vac. Sci. Tech., Part B.

C. D.V. Podlesnik, H.H. Gilgen, and R.M. Osgood, Jr., "Deep Ultraviolet Induced Wet Etching of GaAs," to be published in Appl. Phys. Lett.

D. H.H. Gilgen and R.M. Osgood, Jr., "Electrical Properties of Photodeposited Metal Lines," CLEO 1984, Technical Digest.

E. 1. D.V. Podlesnik, H.H. Gilgen, R.M. Osgood, Jr., and A. Sanchez, "Maskless Chemical Etching of Submicrometer Gratings in Single Crystal GaAs," Appl. Phys. Lett., 43, 1083 (1983).

2. D.V. Podlesnik, H.H. Gilgen, R.M. Osgood, Jr., A. Sanchez, and V. Daneu, "High Resolution Etching of GaAs and CdS Crystals," in Laser Diagnostics and Photochemical Processing for Semiconductor Devices, edited by R.M. Osgood, Jr., S.R.J. Brueck, and H.R. Schlossberg (North-Holland, Amsterdam, 1983).

3. H.H. Gilgen, D.V. Podlesnik, C.J. Chen and R.M. Osgood, Jr., "Direct Holographic Processing Using Laser Chemistry," in Laser-Controlled Chemical Processing of Surfaces, edited by A.W. Johnson, D.J. Ehrlich, (North-Holland, Amsterdam, 1984).

CONFERENCE ON LASERS AND ELECTRO-OPTICS

19-22 JUNE 1984

OSA/IEEE

ANAHEIM, CALIFORNIA

THH4 Electrical properties of photodeposited metal lines

H. H. GILGEN and R. M. OSGOOD, JR., Columbia University, Department of Electrical Engineering, New York, N.Y. 10027.

Metal photodeposition is a local low-temperature thin-film growth process which enables maskless repairing and customization of integrated circuits. Although many of these applications require the writing of good quality conductors, there have been no previous studies of the effect of the deposition conditions on the electrical properties of photodeposited metal lines. Here we report the investigation of the electrical resistivity of photodeposited metal lines under different process parameters.

Our initial experiments were done with cadmium deposited from dimethyl cadmium (DMCd) with the UV light from a frequency-doubled Ar^+ laser onto a glass plate. The plate contained a vacuum evaporated pattern of gold dots. The glass plate was mounted in a static gas cell which was moved with a constant velocity perpendicular to the UV beam. The length, width, and thickness of the lines were determined by microscopy and surface probing. These measurements enabled us to determine the specific resistivity of the lines and to compare these values with those of the bulk. The results for different DMCd pressures with and without buffer gas are shown in Fig. 1(A). The relative resistivity is 4X higher than the bulk resistivity. In addition, in Fig. 1(B) the variation of the resistance with respect to temperature is shown.

In photodeposition, the material growth is dominated by either the decomposition of the adlayer on the surface or the molecules in the gas phase. The structural behavior of the deposited metal which influences the electrical properties is strongly dependent on the growth mechanism. The structures grown preponderantly from the adlayer exhibit light-induced surface ripples, which leads to the increase in resistivity on the low-pressure side of Fig. 1(A). At high DMCd pressure, the growth occurs from a dense metal vapor which causes a coarse-grained nonlocal deposit with increased resistivity [Fig. 1(A)]. At low temperature [Fig. 1(B)], where the adlayer growth dominates, we believe the increased resistivity is due to incomplete adlayer decomposition.

Currently we are performing experiments on other photodeposited metals. These results will be presented.

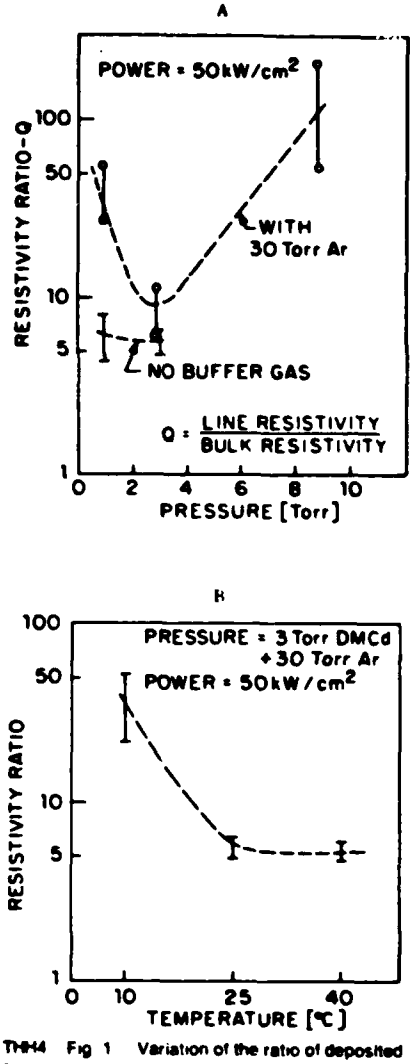

THH4 Fig. 1 Variation of the ratio of deposited film resistivity to bulk resistivity for various deposition conditions: (a) resistivity ratio vs partial pressure of dimethylcadmium, (b) resistivity ratio vs substrate temperature

DIRECT-HOLOGRAPHIC PROCESSING USING LASER CHEMISTRY

H. H. Gilgen, D. Podlesnik, C. J. Chen and R. M. Osgood, Jr.
Department of Electrical Engineering, Columbia University, New York, NY 10027

Abstract

By using two interferring laser beams to initiate localized chemical reactions at an interface, very high resolution, maskless microfabrication can be done over relatively large substrate areas. The resulting deposited or etched patterns can be used in a variety of electrooptical and electronic applications. In addition, this type of fabrication, which can be monitored in real time, provides insight into many new interfacial phenomena.

Introduction

In most of the laser chemical processing described recently, the temporal coherence of the laser source has not played an important role in the processing results or physics.[1] In laser direct writing, for example, the laser spatial coherence plays a key role since it permits submicrometer focusing of the laser beam. In both direct writing and photon-assisted dry processing, the monochromatic nature of the laser is important only in so far as it is necessary to drive a specific chemical channel. Here we will describe a laser chemical processing technique which requires that the light source have a high degree of temporal coherence, namely, laser holographic processing. In this processing, two laser beams are interferred to produce a coherent pattern across a substrate surface. The laser light then by either a linear or nonlinear optical process, such as photodissociation or heating, drives a chemical reaction which causes the necessary local surface alteration.

Our study of laser holographic processing has provided information on both the fabrication of device structures for specific near-term applications and the basic physical phenomena occurring in interfacial chemical reactions. In particular, most of our initial work on holographic processing has emphasized high resolution gratings. These gratings are potentially important for single-wavelength, distributed feedback lasers and for couplers in integrated optics. A novel aspect of this direct fabrication technique is that the gratings can be optically monitored during fabrication which, in turn, allows for precise control over the grating depth and groove profiles. Further, because our gratings have very high resolution, the process of grating fabrication becomes a method for studying the micrometer-scale physical processes which influence the grating structure and growth. These processes may involve, for example, the diffusion of excited species or the magnification of the optical fields at the grating surface.

In this paper, we will illustrate the above aspects of holographic processing by describing two recent experiments in this area: light-enhanced, liquid-phase etching of GaAs and photodeposition of metal from surface layers. In both cases high-resolution gratings have been fabricated and basic physical phenomena observed.

Liquid-Phase Etching of GaAs

The apparatus for this experiment has been described in detail elsewhere.[2,3] Basically, a laser beam from a moderate-power, argon-ion laser passes through a spatial filter and a collimator before being split and mixed inside an optical cell containing an $H_2O_2 : H_2SO_4 : H_2O$ etching solution. The dissolution of GaAs in this solution is influenced by the number of carriers present at the semiconductor surface. For n-type GaAs, photogenerated holes accelerate the etching rate[4], thus forming a photoengraved pattern in the solid surface. Although we have formed high resolution gratings on other III-V as well as on II-VI compound semiconductors, we will limit our discussion here to n-type GaAs doped with Si, $n=10^{18}$ cm^{-3}, and with (100) crystal orientation.

Using the above experimental arrangement, we have produced 130-nm to 200-nm gratings with maximum depth-to-spacing ratios, d/s, of typically 0.2. For gratings with spacings > 1 μm, the depth-to-spacing ratio exceeds 0.4, for example, 2-μm gratings had a ratio of 0.8. The gratings were uniform and without secondary ripples over a relatively large area of ~1 cm^2. This area was limited by the uniformity of the laser beam. The maximum resolution reported here was limited by the wavelength of the laser light. Recently we have used UV radiation to obtain 100-nm period gratings.

In general, the profile of the grating grooves depends on the details of the carrier movement within the semiconductor, the relative magnitude of the dark versus light-enhanced etching rate, and the anisotropy in the etching process. We investigated the profiles of gratings on n-type GaAs for several different crystal orientations using different spacings and etching solutions. For the dilute 1:1:100 solution used in most of our experiments, we found that crystal orientation did not influence the grating profiles and etch rates. Generally, gratings with spacings >1 μm had a sinusoidal profile, see Fig. 1a which is to be expected for a linear dependency between etching rate and light distribution on the surface. On the other hand, submicrometer gratings showed a deviation from a simple sinusoidal profile; typically a cusped profile was observed. Figure 1b shows the development of the characteristic groove-profile for a 300-nm grating. This deviation cannot be explained by a simple theory based on an isotropic diffusion of the holes at the semiconductor surface. Local variations in the hole drift due to photoinduced electric fields, both normal and to the surface transverse to the surface and the interference pattern, give rise to higher-order components in the groove profile, as shown in Fig. 1b.

In general, the etching rate for the submicrometer was found to be dependent on the grating spacing. Figure 2 shows this behavior by displaying the measured depth as a function of the etching time for different grating spacings. The data was obtained by SEM photographs of the GaAs samples cleaved perpendicular to the grooves, however, <u>in situ</u> monitoring, using a He:Ne laser probe, yielded similar data. The slopes of the curves indicate the grating growth rate. In the first 3 to 5 minutes, the gratings grow with a constant rate. For smaller-spacing gratings, i.e. >1 μm, the rate decreases due to the lateral carrier diffusion on the surface. A simplified model[5] gives an expression for carrier distribution, ΔP at a semiconductor surface illuminated with two interferring light beams. In this model, we initially assume a carrier diffusion length in the semiconductor which is smaller than the light absorption depth and a moderate surface recombination. Then,

$$\Delta P = G\left(1 + \frac{s^2}{s^2 + 4\pi^2 L^2} \cos\left(\frac{2\pi x}{s}\right)\right) \qquad (1)$$

where G is a factor proportional to the carrier generation rate, L is the carrier diffusion length in the bulk, s is the grating spacing, and x is direction normal to the grating grooves along the surface. If it is assumed that the local etching rate is proportional to the carrier density, Eq. 1 gives the variation of etching rate with groove spacing. By comparing the measured rates for the different spacings, an approximate diffusion length, L. of 0.12 μm can be obtained. This diffusion length is considerably smaller than the literature value of 1 μm for the GaAs used in our experiment.[6] We believe that this difference can be explained by the strong built-in electric field in the depletion region normal to the interface and the short carrier lifetime at the surface, due to the chemical reaction.

Another feature in Fig. 2 is the decrease in the growth rate of the grating profile for all spacings after about 4 minutes. Separate experiments showed that this decrease cannot be attributed to either a chemical degradation in the etching solution, or to changes in the etching rate with increasing depth in the GaAs samples. We believe that after the grooves attain a specific surface morphology, the photogenerated holes diffuse spatially such that a constant etching rate at each point on the groove profile is maintained. At this point, it is observed that the unmodulated etching continues at a constant rate but the groove profile does not change.

Photodeposition of Metal Gratings

The experiments to investigate photodeposition of metal gratings were accomplished with a 3-5 mW, frequency-doubled, argon-ion laser. This laser has sufficiently short wavelength to photodissociate the metal-alkyl carrier gas, (dimethyl cadmium) used here, and, further, it has an useful temporal coherence length ~20 cm. The laser beam was split and mixed on the rear surface of a quartz flat mounted on a sample-cell containing dimethylcadmium gas. The angle between the two laser beams could be adjusted so as to examine different grating spacings.

Before describing the results obtained here, we point out that high-resolution interference effects have been observed previously for photodeposition.[7] In these cases, it was found that fringes with periods of ~ 0.17 μm could be obtained in photodeposited metal. The origin of these structures has been tied to the stimulated growth of surface plasma waves in a deposit growing from photodeposited parent molecular overlayers. The fringes result from the interference of the surface waves with the incident light. While these fringes are of great scientific interest, their limited coherence length, >2 μm, makes their practical use limited.

With our experimental setup, we readily obtained submicrometer diffraction gratings. In general, the best results were obtained when the sample cell, which contained 10 torr of DMCd and 80 Torr of buffer gas, was cooled to 15° C. At these temperatures physisorbed molecular layers are thick and the contribution from gas-phase photodissociation is minimized. Since the interferring UV beams enter the cell from glass with index n = 1.43, the minimum fringe spacing is

$$p = \frac{1}{n \sin\theta_{max}}$$

where θ_{max} is the maximum angle which we could readily obtain, $\sim 80^{o}$. In fact, grating with periods as small as 300 nm were readily made. Grating formation by photodeposition allows direct optical monitoring of the deposition by a noninvasive optical probe; in our case an He:Ne laser was used. The probe is used by observing the minus-first-order diffracted light from the metal grating. For small modulation depths the intensity of the diffracted light is proportional to h, to the amplitude of the grating ripple. Thus the grating growth rate can be monitored through the rate of increase in the diffracted intensity.

These measurements have shown clearly one of the most striking phenomena associated with optical growth of diffraction gratings. As the angle of interference is varied sharp resonances are observed in the grating growth rates, see Fig 3. These resonances are the result of enhanced coupling of light into surface confined waves within the metal film. The resonances occur when the grating spacing, d, is equal to an odd multiple of half wavelengths of the surface wave which exists at the frequency of the incident optical electric filed, that is, when[8]

$$d(\theta) = 2n + 1 \sqrt{\frac{|\epsilon_1|-1}{|\epsilon_1|}} \lambda_s \qquad (2)$$

where m is an integer, ϵ_1 is the real part of the metal dielectric constant, and λ_s is the wavelength of the unltraviolet light in the quartz window. At the spacing of each resonance the angle one of the diffracted orders is such that the wavevector of the light is just parallel or along the surface of the metal. Thus, each resonance reprsents a spacing such that the amplitude of the surface plasma wave intensity is maximized. Since the local electric field, including incident and scattered waves, determines the rate of grating growth, the deposition is fastest at resonance spacings.

As seen in Fig. 3 the grating growth rate can be increased by as much as a factor of 8 at resonance compared to that for off resonance. For the laser powers and grating areas considered here, this means that relatively dense metallic gratings can easily be grown at resonance, spacings whereas only very thin structures can be obtained at intermediate values.

CONCLUSION

In this paper we have reviewed two forms of holographic photochemical processing. In both cases, the applications were the production of submicrometer diffraction gratings. In both cases unexpected physical phenomena at the interface, control the grating growth rate and resolution.

ACKNOWLEDGEMENT

We would like to thank Antonio Sanchez and S.R.J. Brueck for several helpful comments. This work was supported by the Defense Advanced Research Project Agency, the Air Force Office of Scientific Research, and the Army Research Office.

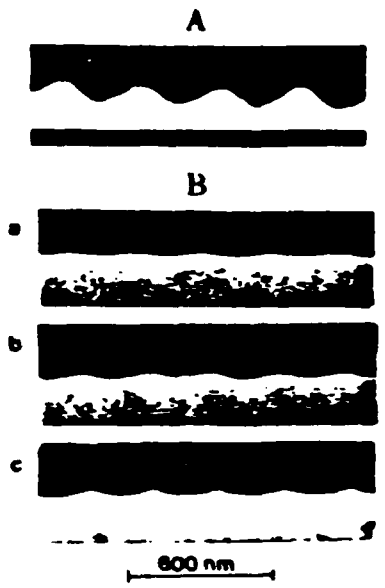

FIG. 1. A) Scanning electron micrographs of gratings with a sinusoidal profile, typical of large spacing, ≥ 1 μm.

B) Micrographs of the groove-profile of 300 nm gratings after etching for top - 1 min., middle - 2 min., and bottom - 3 min. respectively.

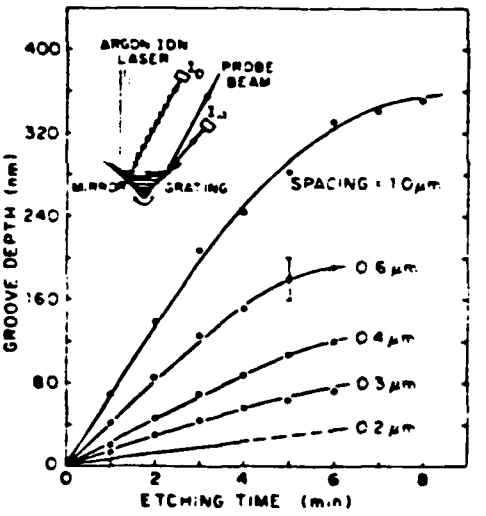

FIG. 2. The measured GaAs - grating-groove depth versus etching time in a 1:1:100 etching solution versus different grating spacings.

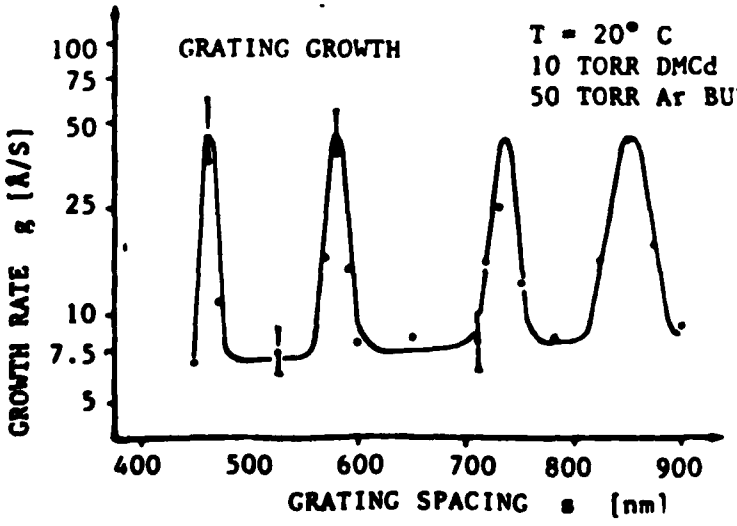

FIG. 3. Growth rate versus grating spacing for metal gratings grown by photo-deposition from adsorbed metal-alkyl molecules with 257 nm light.

REFERENCES

1 R.M. Osgood, S.R.J. Brueck, and H.R. Schlossberg, Laser Diagnostics and Photochemical Processing for Semiconductor Devices, (North Holland, Amsterdam, 1983).

2 R. M. Osgood, A. Sanchez-Rubio, D.J. Ehrlich, and V. Daneu, Appl. Phys Lett., 40, 391 (1982).

3 D. Podlesnik, H.H. Gilgen, R.M. Osgood, and A. Sanchez, Appl. Phys. Lett. (in press).

4 F. Kuhn-Kuhnenfeld, J. Electrochem. Soc., 119, 1063 (1972).

5 L.V. Belyakov, D.N. Goryachev, L.G. Paritskii, S.M. Ryvkin, and O.M. Sreseli, Sov. Phys. Semicond., 10, 678 (1976).

6 H.C. Casey, Jr., B.I. Miller, and E. Pinkas, J. Appl. Phys. 44, 1281.

7 R. M. Osgood and D.J. Ehrlich, Opt. Lett. 7, 385 (1982); R.J. Brueck and D.J. Ehrlich, Phys. Rev. Lett., 48, 1678 (1982).

8 H.H. Gilgen, J. C. Chen, R.M. Osgood, (unpublished).

HIGH RESOLUTION ETCHING OF GaAs AND CdS CRYSTALS*

D. V. PODLESNIK, H.H. GILGEN, R.M. OSGOOD
Department of Electrical Engineering, Columbia University, New York, NY 10027
A. SAWEZ, V. DANEU
MIT Lincoln Laboratory, Lexington, MA 02173

ABSTRACT

Submicrometer gratings have been etched in GaAs and CdS crystals which have been immersed in an oxidizing etch and illuminated with interferring laser beams. A resolution of 170 nm was obtained. At high laser intensity and with prolonged etching time the surface properties of the material are degraded. The use of in-situ optical measurements of grating parameters allows ready optimization of the grating fabrication process.

INTRODUCTION

Recent interest in guided wave optics [1] and distributed feedback lasers [2] has prompted the need for producing gratings with periods on the order of 100 nm on semiconductor materials. Other applications include surface acoustic wave devices [3] and negative-resistance electron devices [4]. Currently, there are two conventional methods for grating fabrication: holographic lithography [5] and electron-beam lithography [6]. With the former method, gratings with spacing as small as 110 nm have been produced; however, this technique is cumbersome, and grating periods are generally restricted to be greater than 180 nm. With electron-beam technique, gratings with the period less than 100 nm can be produced. But, this method is limited by the difficulties of producing uniform large-area structures and the long exposure times, which, for a 300 nm grating, can be as long as one hour per square millimeter [6]. Both methods involve multiple steps. In addition, for both methods, photoresist residues cause contamination problems, limiting their use in electro-optical applications.

In the present paper we describe a technique for producing submicrometer gratings by a holographic method with direct chemical etching in an oxidizing etch [7]. The resolution of this technique is comparable to those of other methods. Futhermore, this method is a single one-step process using very low laser intensity. Both uniform large-area gratings and special grating profiles (e.g. blazed) can be easily fabricated.

The anodic dissolution of a semiconductor in an oxidizing etch is generally influenced by the number of carriers present at the surface. Since light incident on the semiconductor surface produces electron-hole pairs, a pattern of light produces a corresponding pattern of available carriers. The photogenerated carriers, typically holes for n-type GaAs, control the etching rate of a semiconductor producing an engraved pattern in its surface. The resolution of the etching process may be shown to be a direct consequence of rapid surface recombination velocity, due to the etching reaction, and the surface-normal electric field, due to the semiconductor band bending at the interface. Our results show that 170 nm gratings are easily obtained and we anticipate that with an appropriate optical arrangement, a resolution below 100 nm is possible.

Mat. Res. Soc. Symp. Proc. Vol. 17 (1983)

EXPERIMENT

The actual experimental arrangement used for the holographic exposure is shown in Fig. 1. A laser beam from an argon-ion laser emitting at 514.5, 488.0, or 457.9 nm passes through a spatial filter. The filtered beam is incident on a right angle corner on which are mounted a mirror and a semiconductor sample. The corner is inside an optical cell containing an etching solution. The interference pattern is produced by the superposition of the direct and the reflected beams inside the solution. The grating period, s, is given by

$$s = \frac{\lambda}{2\, n \sin\theta_i} \tag{1}$$

where λ is the free-space wavelength of incident light, n is the index of refraction of the solution and θ_i is the incident angle on the sample surface. The incident light is s-polarized. After passing through the spatial filter, the laser beam goes through the window of the optical cell, and it is, therefore, desirable to match as much as possible the indices of refraction of the solution and the window in order to reduce spurious interference patterns.

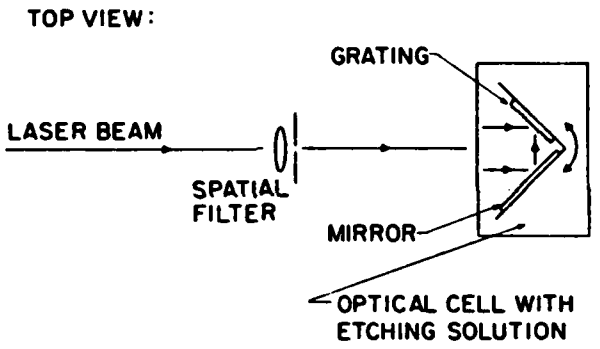

Fig. 1 Experimental arrangement for grating fabrication by direct chemical etching

The experiment was done on GaAs and CdS crystals. A comparison was made of etching gratings on n(10^{18} cm^{-7}) and SI GaAs of (100) and (111) orientations. On all samples, good quality and small-period gratings were produced. Figure 2 shows a SEM photograph of 200-nm grating on n-type GaAs. Using 457.9 nm line we have recently obtained gratings with a 170 -nm period. Successful gratings on CdS (undoped) were produced only on prismatic faces, parallel to the optical axes, as shown on Fig. 3. We failed to produce good quality gratings on A and B CdS faces.

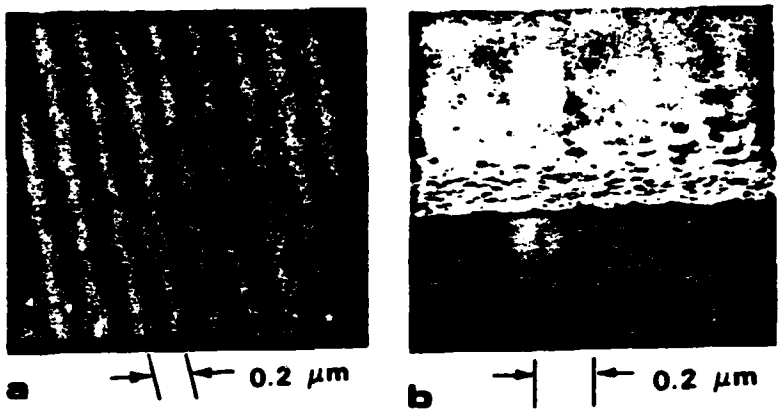

Fig. 2 The SEM photographs of a 200-nm grating on n-type GaAs. Fig. (a) shows the top view of the (100) surface and Fig. (b) shows the profile of the grating.

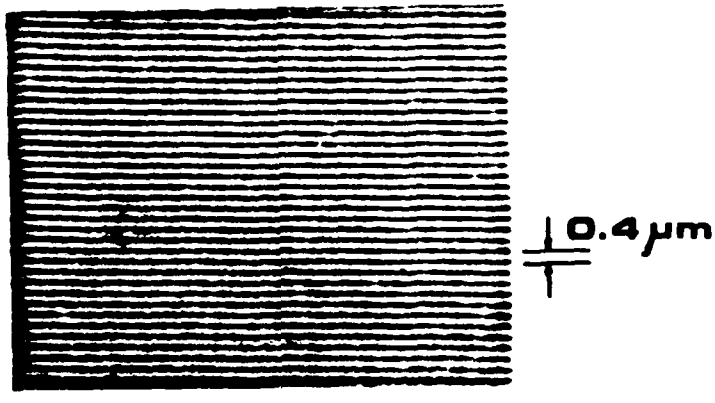

Fig. 3 The photograph of the grating formed on a prismatic face of CdS (undoped). The periodicity is about 400 nm.

Although several different etching solutions (e.g. NH_4OH, H_2O_2, and H_2O, or KCl, HCl, and H_2O) were used, most of the work was done with the following solution: H_2SO_4, H_2O_2 and H_2O [8]. Since we were primarily concerned with grating periods less than 400 nm, it was necessary to choose an etch composition with a sufficiently slow dark etching rate, that the products of the etching reaction would not interfere with the development of the grating. Based on an initial measurement of the dark and light-enhanced etching rates for different compositions, we selected the following composition for our experiments: H_2SO_4: H_2O_2: H_2O = 1:1:50.

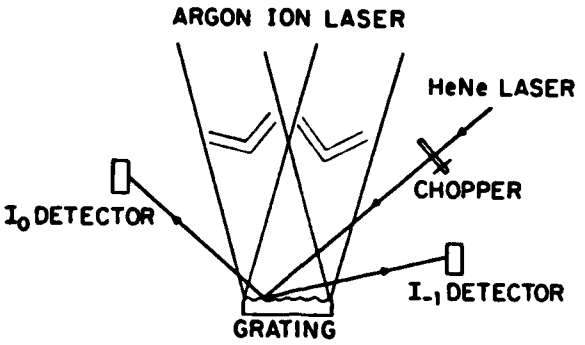

Fig. 4 Experimental arrangement for the in-situ measurement.

OPTICAL MEASUREMENT OF GRATING PARAMETERS

The in-situ measurement enabled us to observe the quality of the etched surface and determine grating parameters during the etching process. This provides a convenient means of studying the fabrication process and it has allowed the optimization of the process parameters. The in-situ measurement arrangement is represented in Fig. 4. The probe was a HeNe laser, operating at 633 nm. In order to minimize etching with the output from the HeNe laser, the beam was attenuated and chopped with a small duty cycle. The intensities of diffracted beams were measured with a power meter. For small period gratings, measured here, $\sim$ 400 nm, the relatively long wavelength of the probe-beam allowed only diffraction of the zero and the minus first order .

To determine the important parameters of the grating, the spacing, s, and the groove depth, d, we measured the angular position θ_{-1} and the relative intensity of the minus first diffraction order, I_{-1}/I_{00}, when the sample is irradiated with s-polarized light at the angle of incidence θ_i. The diffraction angle θ_{-1} is related to θ_i by

$$\sin \theta_{-1} = \frac{\lambda_p}{n\, s} - \sin \theta_i \qquad (2)$$

where λ_p is the free-space wavelength of the probe beam. If I_{00} is the intensity of the beam reflected from the polished crystal surface (taken as 100%), the theoretical value [9] of the intensity of the minus first order as a function of the grating depth, d, is given by

$$\frac{I_{-1}}{I_{00}} = J_1^2\left(\frac{2\pi n\, d}{\lambda_p}\,(1+\cos\theta_{-1})\right) \qquad (3)$$

where J_1 is the Bessel function of the first kind, order one. Here we assumed that the grating surface is purely sinusoidally corrugated. As one can see (Fig. 2), our gratings showed the deviation from the sinusoidal curvature, but we can use Eq. 3 as an approximation to estimate the grating depth. An exact calculation requires the Fourier expansion of the surface corrugation.

Figure 5 shows the dependence of the relative specular reflection intensity I_0/I_{00} on the exposure time (etching time). During the measurement we used only a single non-interfering argon-ion laser beam. As a result we obtained information about the scale of roughness that occurs when the sample is immersed in the solution. One can observe the surface degradation under different light intensities with prolonged etching time. The results indicate that the growth rate of the statistical surface roughness depends on the laser intensity.

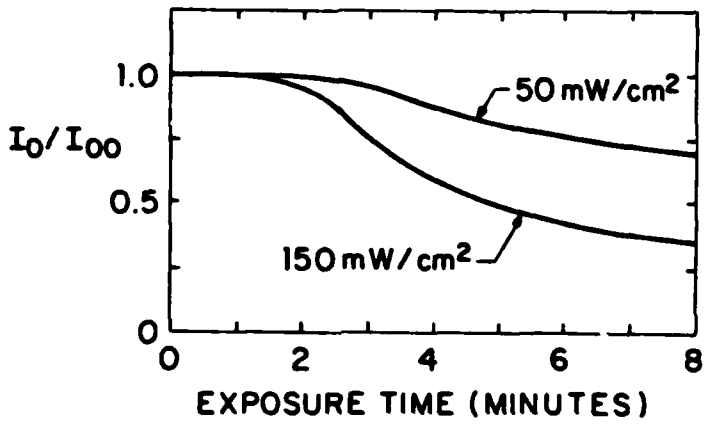

Fig. 5 The normalized intensity, I_0/I_{00}, of the reflected HeNe beam from the GaAs surface during the etching process as a function of the exposure time. Results for two different laser intensities are shown.

The relative intensity of the minus first diffraction order, I_{-1}/I_{00}, has been measured as a function of the exposure time. The results for two different incident laser powers are given in Fig. 6. We found that at the beginning of the grating growth the exposure time is proportional to the grating depth, assuming a constant etching rate. Thus, at the beginning, the growth of a good quality grating is observed, since the relative intensity I_{-1}/I_{00} follows the appropriate Bessel function. The later decrease of I_{-1}/I_{00} is related to the statistical roughness of the etched surface (see Fig. 5) and to a change of the etching rate. The proportionality of the exposure time and the grating depth is not valid in this region. In our example we found that the exposure time of 90 seconds was optimal, giving the grating depth of about 160 nm.

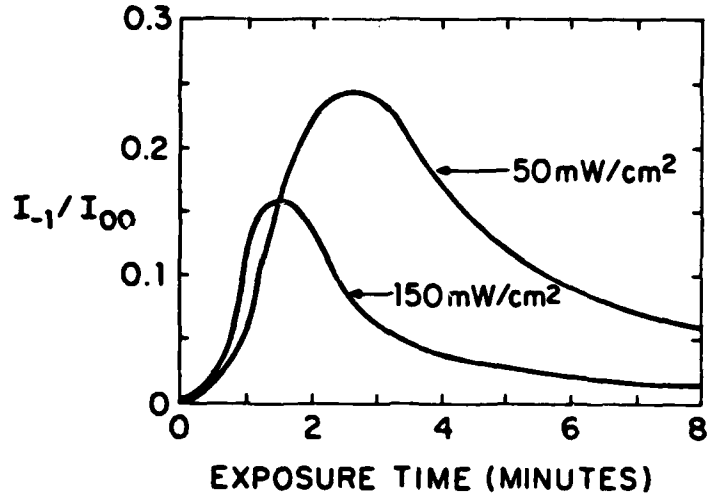

Fig. 6 Relative intensities of the minus first diffraction order vs the exposure time. The diffraction is from the n-type GaAs surface during the fabrication of a 400-nm grating.

From the Fig. 6, we can also observe the effect of laser-light intensity. At a higher intensity the etching rate is higher, but the surface degradation is faster and stronger. For the intensities above 1 W/cm^2 we even observed total distruction of gratings. For our experimental conditions the optimal laser intensities were between 10 and 50 mW/cm^2.

CONCLUSION

We have demonstrated a technique for producing a high-resolution periodic structure on compound semiconductors. Gratings with the spacing of 170 nm were produced. The method is distinguished by simplicity and efficiency. Optical measurements of grating parameters during the etching make the process optimization possible.

ACKNOWLEDGEMENTS

We would like to thank Professors G.W. Flynn and S.P. Schlesinge. for their encouragement and support. In a dition, we benefited from discussions with Dr. A. Szöke and Professor E.S. Y g.

*This work was supported by the Defense Advanced Research Projects Agency and the Air Force Office of Scientific Research.

REFERENCES

1. P.K. Tien, Rev. Mod Phys., 49, 361 (1977).

2. A. Yariv and H. Nakamura, IEEE J. Quantum Electron, QE-13, 233 (1977).

3. R.C. Williams, H. I. Smith, Elect. Lett. 8, 401 (1972).

4. H. Sakaki, K. Wagatsuma, J. Hamasaki, and S. Saito, Thin Solid Films, 36, 497 (1976).

5. C.V. Shank and R.V. Schmidt, Appl. Phys. Lett. 23, 154 (1973).

6. H.I. Smith, Proc. of the IEEE, 1361 (October 1974).

7. R.M. Osgood, A. Sanchez-Rubio, D.J. Ehrlich, and V.Daneu, Appl. Phys. Lett. 40, 391 (1982).

8. S. Ida and K. Ito, J. Electrochem. Soc. 118, 768 (1971).

9. I. Poekrand and H. Raether, Opt. Commun. 18, 395 (1976).

Maskless, chemical etching of submicrometer gratings in single-crystalline GaAs

D. V. Podlesnik, H. H. Gilgen, and R. M. Osgood, Jr.
Department of Electrical Engineering and Columbia Radiation Laboratory, Columbia University, New York, New York 10027

A. Sanchez
MIT Lincoln Laboratory, Lexington, Massachusetts 02173

(Received 8 August 1983; accepted for publication 23 September 1983)

Submicrometer optical gratings are produced in a GaAs surface by a laser enhanced, wet-etching process which permits the fabrication of different grating profiles. The etch process was investigated by *in situ* optical measurements of the diffracted beams and electron microscopy.

PACS numbers: 81.60. – j, 42.80.Fn

High-resolution optical gratings with periods between 100 and 300 nm are required for many electro-optical devices of III-V compounds.[1] In the case of optical couplers, the gratings must be blazed to be efficient. It has been previously shown[2,3] that laser-enhanced liquid etching is a simple and convenient method for fabrication of semiconductor gratings with spacings, from the hundred micrometer to the micrometer range. Since this method is simple and direct, i.e., maskless, it has advantages over conventional lithographic techniques.[4,5] Here, we report on fabricating ultrahigh resolution gratings, ~ 200 nm, with controllable and reproducible optical properties. Furthermore, we show that under different conditions a variety of groove profiles, including blazed, sinusoidal, and "impulse" shapes, can be made.

An important feature of the direct etching process is that the parameters of gratings can be monitored during fabrication.[3] Using *in situ* optical measurements of grating parameters, an optimization of the etching process for different semiconductor-electrolyte systems is possible. In addition, the *in situ* measurement provides data on the ultimate resolution and physics of the liquid etching processes.

The experimental arrangement used is simple, mechanically stable, and is readily adjusted to obtain a wide range of grating spacings[3] (see insert Fig. 1). A laser beam from a moderate-power argon-ion laser passes through a spatial filter and a collimator before impinging on a right-angle corner. The corner, on which a mirror and a semiconductor sample are mounted, is inside an optical cell containing an H_2O_2:H_2SO_4:H_2O etching solution. An interference pattern is produced by the superposition of the direct and the reflected beams inside the solution, which has an index of refraction greater than one, approximately 1.33, due to the high water content. The dissolution of GaAs in this solution is influenced by the number of carriers present at the semiconductor surface. For *n*-type GaAs, photogenerated holes accelerate the etching rate[6] thus forming a photoengraved pattern in the solid surface. Although we have formed high resolution gratings on other III-V as well as on II-VI compound semiconductors, we confine our attention in this letter to *n*-type GaAs doped with Si, $n = 10^{18}$ cm^{-3}, and with (100) crystal orientation. The grating grooves were generally made parallel to the [110] direction.

In order to perform *in situ* monitoring, a beam splitter was inserted in the optical train of the main beam to "split off" a probe beam. The probe beam was further attenuated and chopped at a small duty cycle in order to avoid unwanted etching. The diffracted light (see insert in Fig. 1), which was measured with a commercial power meter, can then be related to the groove depth and profile. Detailed groove profiles were measured with a scanning electron microscope (SEM). The argon-ion laser was operated in one of two lines: 514.5 or 457.9 nm. The maximum laser intensity was 700 mW/cm^2; however, 300 mW/cm^2 was the typical intensity used in the experiments. Notice that for this range of laser intensity, thermal effects, either in the solution or on the semiconductor surface, can be neglected.

For example, in Table I we compare different ratios between unmodulated etching and grating etching rates for two etching solutions. As Table I shows the etching solution with the best performance for gratings with resolution better than 600 nm was H_2O_2:H_2SO_4:H_2O = 1:1:100. Similar results were found by measuring the optical quality of gratings. Typically, the etching time was between 2 and 6 min. Using the above experimental arrangement we have produced 170- and 200-nm gratings with maximum depth-to-spacing ratios d/s of typically 0.2; e.g., for the 200-nm grating a depth of 40 nm was observed. For gratings with spacings > 1 μm, the depth-to-spacing ratio exceeds 0.4; for example, the 2-μm gratings had a ratio of 0.8. The gratings were uniform and without secondary ripples over a relatively large area of ~ 1 cm^2. This area was limited by the uniformity of the laser beam. The maximum resolution reported here was limited

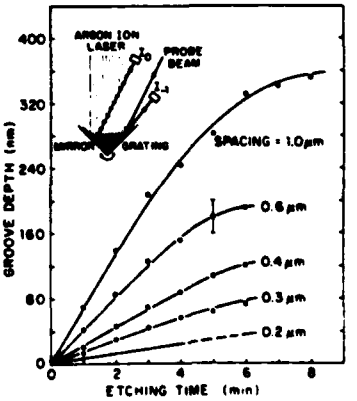

FIG. 1. Measured grating-groove depth vs the etching time in an 1:1:100 solution for different grating spacings. The points are evaluated by SEM measurement. The curve for the 200-nm grating is obtained by *in situ* measurements. The insert shows a part of the experimental arrangement.

TABLE I. Ratios between unmodulated etching rate and grating growth rate for two different solutions. Despite the large difference in the ratio between the 1- and 0.2-μm gratings the grating formation time for the maximum observed depth is comparable for these two grating spacings, as shown in Fig. 1 for solution (b). Unmodulated etching rate is 0.5 μm/min for solution (a), and 0.2 μm/min for solution (b).

Grating spacing (μm)	Ratio for 1 : 1 : 25 solution (a)	Ratio for 1 : 1 : 100 solution (b)
1.0	0.20	0.25
0.6	0.12	0.20
0.3	0.02	0.08
0.2	0.008	0.03

only by the wavelength of the laser light; in a separate series of experiments we have used UV radiation to obtain even smaller periods.

In general, the etching rates for the submicrometer gratings were found to be dependent on the grating spacing. Figure 1 shows this behavior by displaying the measured depth as function of the etching time for different grating spacings. The data were obtained by SEM photographs of the GaAs samples cleaved perpendicular to the grooves. The slopes of the curves indicate the grating growth rate. In the first 3–5 min the gratings grow with a constant rate. For smaller-spacing gratings, i.e., <1 μm, the rate decreases due to the lateral carrier diffusion on the surface. A simplified model gives an expression[7] for carrier distribution ΔP at a semiconductor surface illuminated with two interfering light beams. In this model we initially assume a carrier diffusion length in the semiconductor which is smaller than the light absorption depth and a moderate surface recombination. Then,

$$\Delta P = G\left[1 + \frac{s^2}{s^2 + 4\pi^2 L^2}\cos\left(\frac{2\pi x}{s}\right)\right], \tag{1}$$

where G is a factor proportional to the carrier generation rate, L the carrier diffusion length in the bulk, s the grating spacing, and x the direction normal to the grating grooves along the surface. If it is assumed that the local etching rate is proportional to the carrier density, Eq. (1) gives the variation of etching rate with groove spacing. By comparing the measured rates for the different spacings, an approximate diffusion length L of 0.12 μm can be obtained. This diffusion length is considerably smaller than the literature value of 1 μm for the GaAs (Ref. 8) used in our experiment. We believe that this difference can be explained by the strong built-in electric field in the depletion region normal to the interface and the short carrier lifetime at the surface, due to the chemical reaction.

Another feature in Fig. 1 is the decrease in the growth rate of the grating profile for all spacings after about 4 min. Separate experiments showed that this decrease cannot be attributed to either a chemical degradation in the etching solution, nor changes in the etching rate with increasing depth in the GaAs samples. We believe that after the grooves attain a specific surface morphology, the photogenerated holes diffuse spatially such that a constant etching rate at each point on the groove profile in maintained. At this point, it is observed that the unmodulated etching continues at a constant rate but the groove profile does not change.

In general, the profile of the grating grooves depends on the details of the carrier movement within the semiconductor, the relative magnitude of the dark versus light-enhanced etching rate, and the anisotropy in the etching process. We investigated the profiles of gratings on n-type GaAs for several different crystal orientations using different spacings and etching solutions. For the dilute 1:1:100 solution used in the experiments, we found that crystal orientation did not influence the grating profiles and etch rates. Generally, gratings with spacings >1 μm had a sinusoidal profile [see Fig. 3(a)], which is to be expected for a linear dependency between etching rate and light distribution on the surface. On the other hand, submicrometer gratings showed a deviation from simple sinusoidal profile; typically a cusped profile was observed. Figure 2 shows the development of characteristic groove profile for a 300-nm grating. This deviation cannot be explained by a simple theory based on an isotropic diffusion of the holes at the semiconductor surface. Local variations in the hole drift due to photoinduced electric fields, both normal and transverse to the surface and the interference patterns, give rise to higher order components in the groove profile, as shown in Fig. 2.

Because of the practical importance of blazed gratings we have developed a simple technique for their fabrication. The approach was to tilt the semiconductor substrate so that the bisector of the angle of the interference was at an angle with respect to the surface normal. This tilting was accomplished by mounting the substrate on a non-right-angle corner; the deviation from 90° represents the blazed angle. The tilting of the substrate in conjunction with the continuous

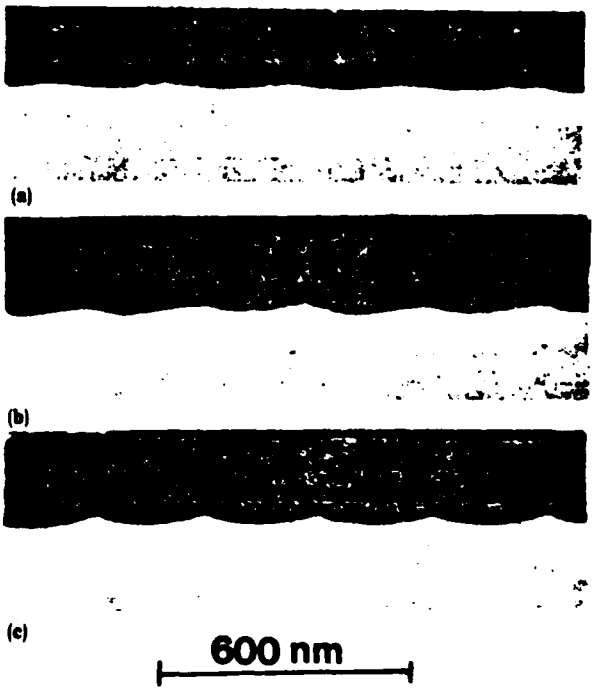

FIG. 2. SEM micrographs of the groove profile for 300-nm gratings on GaAs after different etching times in the 1:1:100 solution. The etching time was (a) 1 min, (b) 2 min, and (c) 3 min.

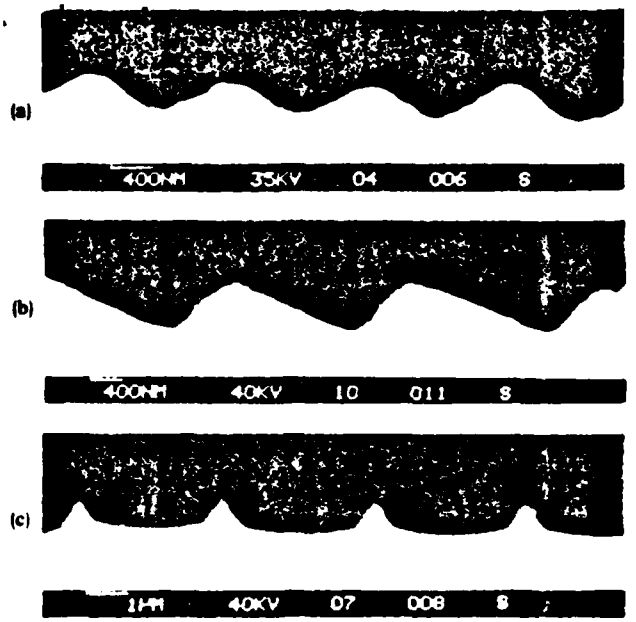

FIG. 3. SEM micrographs of gratings with (a) sinusoidal, (b) blazed, and (c) "impulse" profile.

dark etching, which progresses normal to the surface, produces a clear, blazed profile, as shown in Fig. 3(b). The profile can be triangular or cusped depending on the relative magnitude of the uniform and light-enhanced etching rate.

More unusual grating profiles could be produced under extreme conditions of etching. For example, using a solution with a 10 times higher H_2O_2 content than the value quoted above and a laser power density of 1 kW/cm^2, we produced a 3-μm impulse grating whose profile was a series of narrow peaks [see Fig. 3(c)]. We believe that the extremely fast etching rates under these conditions had a strong anisotropic nature which caused this particular profile.[9]

An important dimension of the direct optical fabrication is that the growth of the grating can be monitored during the fabrication process. In the case described here the grating properties can be monitored by observing the zeroeth or minus first order I_{-1} diffracted light from the probe beam (see insert Fig. 1). Theoretical treatments of a simple sinusoidal grating have shown that the ratio of the minus first order diffracted and the initially reflected I_{00} beams is given by[10]

$$I_{-1}/I_{00} = J_1^2[(2\pi nd/\lambda)(1+\cos\theta_{-1})] \qquad (2)$$

where d is the depth of the grating grooves, λ the free-space wavelength of the probe beam, n the index of refraction of the solution, and θ_{-1} the angular position of minus first order. For a nonsinusoidal grating, such as observed for spacings $< 1\,\mu$m, this relation still gives a good approximation for shallow gratings. From the position of the first maximum of the Bessel function, the grating growth rate can be determined within an accuracy better than 10%. However, Eq. (2) is inadequate for deeper grating profiles, as numerical simulations and experimental results have shown. In that case the magnitude and shape are strongly dependent on the groove profiles. Notice that by monitoring the I_{-1} intensity it is possible to obtain a direct and *in situ* control of the fundamental grating characteristics.

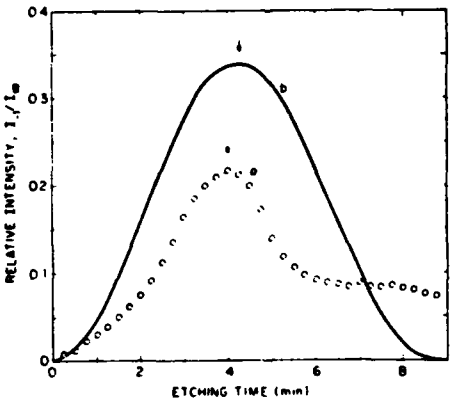

FIG. 4. Relative intensity of the minus-first-order diffracted beam, I_{-1}/I_{in} (a), from a 300-nm grating as function of the etching time. For comparison the theoretical curve (b) evaluated by Eq. (2) is inserted.

Figure 4 shows the measured ratio I_{-1}/I_{00} as a function of the etching time for a 0.3-μm grating. A curve calculated from Eq. (2) using the constant grating growth rate, given in Fig. 1, is included on the same plot. The agreement in the overall shape of the curves is excellent. Note, however, that the measured curve does not drop completely to zero at the largest time point shown. This behavior reflects the saturation in the etching rate shown in Fig. 1, thus precluding a total "zeroing" of the I_{-1} intensity as predicted by Eq. (2). For long etching times, not shown in Fig. 4, the groove profiles degrade due to random surface material defects and beam inhomogeneity.

The experimental results given here indicate that submicrometer gratings with s/d ratios of 0.2 to 0.8 can be precisely fabricated in GaAs using laser chemical etching with *in situ* monitoring. The groove profiles and growth rate for different spacings indicates that the chief limitation on process resolution in the visible wavelength range is the diffusion of carriers produced below the semiconductor surface. Shorter laser-wavelength radiation, which has smaller optical penetration depth, would alleviate this limitation.

Finally, we would like to thank Joan Whelan and Paul McGuffin for help in the SEM measurements, and Peter Brewer, Julian Chen, and Vincenzo Daneu for many helpful discussions. This work was supported by the Defence Advanced Research Project Agency and the Air Force Office of Scientific Research.

[1] A. Yariv and H. Nakamura, IEEE J. Quantum Electron. QE-13, 233 (1977).
[2] R. M. Osgood, A. Sanchez-Rubio, D. J. Ehrlich, and V. Daneu, Appl. Phys. Lett. 40, 391 (1982).
[3] D. V. Podlesnik, H. H. Gilgen, R. M. Osgood, A. Sanchez, and V. Daneu, in *Laser Diagnostics and Photochemical Processing for Semiconductor Devices*, edited by R. M. Osgood, S. R. J. Brueck, and H. R. Schlossberg (North-Holland, Amsterdam, 1983), p. 57.
[4] C. V. Shank and R. V. Schmidt, Appl. Phys. Lett. 23, 154 (1973).
[5] H. I. Smith, Proc. IEEE 62, 1361 (1974).
[6] F. Kuhn-Kuhnenfeld, J. Electrochem. Soc. 119, 1063 (1972).
[7] L. V. Belyakov, D. N. Goryachev, L. G. Paritskii, S. M. Ryvkin, and O. M. Sreseli, Sov. Phys. Semicond. 10, 678 (1976).
[8] H. C. Casey, Jr., B. I. Miller, and E. Pinkas, J. Appl. Phys. 44, 1281 (1973).
[9] S. Ida and K. Ito, J. Electrochem. Soc. 118, 768 (1971).
[10] I. Pockrand and H. Roethen, Opt. Commun. 18, 395 (1976).

Deep-ultraviolet Induced Wet Etching of GaAs

D.V. Podlesnik, H.H. Gilgen, R.M. Osgood, Jr.
Department of Electrical Engineering
and
Columbia Radiation Laboratory
Columbia University
New York, New York 10027

Abstract

We report on deep-ultraviolet (UV), light-assisted wet etching of GaAs. The etching chemistry differs from that using visible wavelengths and all doping types of GaAs can be efficiently etched. The UV processing offers rapid etching at low, nonthermal laser intensities and permits very deep, vertical features to be made.

Light-enhanced, electrodless, wet etching has been sucessfully used for maskless patterning of compound semiconductors. Typically, the photogenerated minority carriers at the semiconductor-solution interface induce or accelerate the etching, thus forming a photoengraved pattern in the solid surface.[1] Recently, this technique was used in conjunction with laser interferometry to fabricate ultrahigh-resolution gratings on GaAs with controlled groove profiles.[2,3] In that, and in most of the previously reported experiments with compound semiconductors,[4-6] visible or near-UV light was used to irradiate the semiconductor samples mounted in the etching solution.

In this letter, we describe a series of experiments in which we have used deep-ultraviolet laser light for fast, maskless wet etching of GaAs, including n, p, and semiinsulating (SI) substrates with (100) orientation. For all doping types, the etch rates, at low laser intensities, were higher in the deep-ultraviolet than in the visible. This rapid, room temperature etching process has enabled us to etch, for example, micrometer-scale via-holes with perfectly vertical walls, through a standard GaAs wafer. We attribute the rapid etching rates to the interfacial chemistry which occurs when deep-UV radiation illuminates a semiconductor surface in an aqueous solution.

For the etching experiments in the ultraviolet, the 257-nm output from a frequency-doubled Ar^+ laser was used. The comparison with etching at visible wavelengths was done with the fundamental 514-nm line. The laser power, incident on the GaAs surface ranged from 50 mW/cm^2 to 2 kW/cm^2. The laser light was coupled into a microscope and focused to a 4-5 μm spot on the GaAs surface. The semiconductor sample

was mounted inside a quartz cell, filled with an etching solution, in such a position that the light path through the liquid was ~ 400 μm. Using a computer-controlled, microscope stage, we could scan the sample perpendicular to the axis of the laser beam. In order to determine the quality and the depth of etched structures, the semiconductor was cleaved precisely across the etched structures. The cross-section of the etched features were investigated with an optical microscope or, in some cases, with a scanning-electron microscope (SEM). Also, a stylus profilometer was used to measure the depth of shallow, etched structures.

For the measurements described in this letter we used three doping types of (100) GaAs - Si-doped ($n=10^{18}$ cm^{-3}), Cr-doped (resistivity $>10^{7}$ Ω-cm), and Zn-doped ($p=10^{18}$ cm^{-3}). Also, three different aqueous solutions were examined, one tertiary solution, H_2SO_4 : H_2O_2 : H_2O, and two binary solutions, HNO_3 : H_2O, and KOH : H_2O. Etching solutions were diluted, so as to have small or no dark etching. The specific reagent compositions were 97% H_2SO_4, 30% H_2O_2 and 70% HNO_3 by volume, and 85% KOH by weight.

The solutions used in our experiments did not exhibit strong UV activation of the bulk liquid. Such an effect would be deterious for the high resolution, maskless etching. Bulk activation was, however, observed for higher-concentration solutions,[7] e.g. 4% H_2O_2 or 10% HNO_3, by volume. In these cases weak nonlocalized etching was observed up to several millimeters from the focused spot. In general, we find that such delocalized etching correlates well with the degree of UV absorption in the etching solution.

Figure 1 shows the etch rates for n-type GaAs in different etching solutions as a function of UV or visible light intensity. A typical

The difference in UV and visible light etching in the low intensity region of Fig. 1 cannot be explained by the fact that more minority carriers are created close to the surface under UV than under visible illumination. It is known that for n-type GaAs the photogenerated holes are driven to the surface by the electric field, which is due to the band bending in the semiconductor.[10] For the doping level used here, 10^{18} cm^{-3}, the electric-field-region depth[11] is estimated to be 30 nm. A comparison with the light-penetration in GaAs for the visible[12] (100 nm) and the ultraviolet[12] (5 nm) clearly shows that only in the ultraviolet, will all photogenerated holes be driven to the surface by the electric field prior to recombination. However, because of the higher energy per photon and the increased reflection in the UV,[12] the total volumetric hole production per unit incident laser intensity is smaller than in the visible. Thus, for equal laser intensities, approximately the same number of holes will reach the surface, for both visible and UV illumination.

The observations at low laser intens. .es suggest that the basic interface chemistry is changed under UV-illumination. For example, the observed chemical activation of deionized water requires injection of holes from GaAs to the H_2O/O_2 redox level. This level is located $\sim$0.4 eV below the top of the GaAs valence band.[13] Thermalized holes in the valence band are not able to access this redox level and to activate the reaction; thus, we require hot, nonthermalized holes at the GaAs water interface to obtain this particular chemical reaction. In fact, previous experiments have shown that hot electrons are active in promoting surface chemical reactions.[14] It is reasonable, therefore, that the hot holes, excited in GaAs will cause the oxidation reaction observed here.

In GaAs crystals, the visible light photons are absorbed by the electron transitions in the center of the Brillouin zone and the excess photoenergy is transfered to electrons only; further, most carriers are created deep in the semiconductor and, thus, energy relaxation occurs during diffusion to the surface. However, the 257-nm photons induce a transition at the X-edge of the Brillouin zone[15] and the UV-generated holes are created deep, ~2.5 eV, below the top of the valence band. Since these holes are produced within 5 nm from the liquid-solid interface, energy relaxation is incomplete for carriers reaching the surface. Using a physical model[16] and rate data[17] for hot electrons in GaAs, we conservatively estimate that the corresponding energy relaxation time for holes in our experiment is 10^{-12}s. This is considerably longer than the transit time, $\tau_t \approx 10^{-13}$s,[18] through the laser illuminated layer on the GaAs surface. This estimation predicts that most of the photoexcited holes would reach the solid-liquid interface with enough excess-energy to access, for example, the H_2O/O_2 redox level. A more accurate calculation will need a detailed model for the recombination and transport of UV-generated carriers.

Despite the fact that the enhanced etching rate is not directly attributable to the very small optical absorption depth in the UV, the fact that carriers are produced virtually on the GaAs surface influences two major etching characteristics. First, the process resolution which depends on the carrier diffusion towards and in the interface region of the semiconductor, is increased. For visible light[2,3] this resolution limit is about 200 nm. We have recently shown that by using 257-nm light in conjunction with the holographic set-up discussed elsewhere,[2] 100-nm gratings with good quality can be produced;[7] second, that all

three doping types of GaAs can be readily etched in a wide variety of etching solution, see Table I. Generally, the difference in etching rates between n-type, SI, and p-type materials is attributable to the difference in the carrier-collection efficiency. In p-type GaAs for example, the band-bending electric field drives the photogenerated holes away from semiconductor surface, whereas in n-type material the opposite is true. Only holes, generated in the first 3-4 atomic layers can reach the semiconductor surface by a random, thermal motion. We estimate that ~5% of the UV-generated holes will reach the surface in p-type GaAs. This number is in good agreement with the measured etch rate. This agreement also indicates that the injection of hot holes in the solution is very rapid and is not the rate limiting step.

Rapid and well-resolved etching in dilute solutions and at low laser intensities suggests that high-quality via-holes, which are important for fast microwave devices and micromachining in general, can be etched in GaAs crystals. This possibility was investigated in a series of experiments in which the laser light was focused on n-type GaAs. By monitoring the via-hole formation and examining the cleaved cross sections, it was found that the etching slowed down as the hole depth increased, particularly at high laser intensities. This effect limits the wafer thickness which can be etched at a particular incident intensity. For high laser intensity the etching process begins rapidly but stops completely after ~100 μm. At this intensity (≥ 1 kW/cm^2), scattered and reflected light inside the hole degrades the wall quality, and prevents further penetration. For lower intensities, the hole-etching rate is slower, but more penetrating, resulting in deep, high-quality via-holes, Fig. 2. The entrance and the exit of the etched via-

hole, Fig. 2 , are well defined and the surrounding area is undamaged. Another remarkable feature of these via-holes, is their perfectly vertical walls, Fig. 2(b), which can be attributed to "waveguiding" of the etching beam. At 100 mW/cm^2, we were able to etch a 1- μm-diameter hole through a 100- μm-thick GaAs sample; at somewhat higher powers we were able to bore through a standard 250- μm wafer although larger, 4- μm diameter hole resulted.

In summary, we report the use of deep UV laser light to drive liquid-phase etching of all doping forms of GaAs. The ultraviolet radiation initiates a different type of interface chemistry than visible light; we believe that the rapid etching at low laser intensities originates from hot carriers injected in the solution. The etching process is rapid and capable of producing high spatial resolution and large aspect ratios.

We would like to acknowledge several important and useful suggestions by Drs. R. Salathe, W. Hwang, A. Sanchez and D. Auston, and thank T. Cacouris for expert technical assistance. This work was supported by the Defense Advanced Research Project Agency and the Air Force Office of Scientific Research.

References

1. F. Kuhn-Kuhnenfeld, J. Electrochem. Soc. 119, 1063 (1972).

2. D.V. Podlesnik, H.H. Gilgen, R.M. Osgood, A. Sanchez, and V. Daneu, in Laser Diagnostics and Photochemical Processing for Semiconductor Devices, edited by R.M. Osgood, S.R.J. Brueck, and H.R. Schlossberg (North-Holland, Amsterdam, 1983), p. 57.

3. D.V. Podlesnik, H.H. Gilgen, and R.M. Osgood, Appl. Phys. Lett. 43, 1083 (1983).

4. G.C. Tisone and A. Wayne Johnson, Appl. Phys. Lett. 42, 530 (1983).

5. S. Mottet and L. Henry, J. Physique 44, C5-139 (1983).

6. R.M. Osgood, A. Sanchez-Rubio, D.J. Ehrlich, and V. Daneu, Appl. Phys. Lett. 40, 391 (1982).

7. D.V. Podlesnik, H.H. Gilgen, and R.M. Osgood, in Laser-Controlled Chemical Processing of Surfaces, edited by A.W. Johnson, D.J. Ehrlich (North-Holland, Amsterdam, 1984), p.82.

8. J. Van Muylder and M. Pourbaix, in Atlas of Electrochemical Equilibria in Aqueous Solutions (National Association of Corrosion Engineers, Houston, 1974), p. 521.

9. C. Vanleugenhaghe, N. de Zoubov, and M. Pourbaix, in Atlas of Electrochemical Equilibria in Aqueous Solutions (National Association of Croorosion Engineers, Houston, 1974), p. 434.

10. H. Gerischer, J. Electroanal. Chem. 58, 263 (1975).

11. S.M. Sze, Physics of Semiconductor Devices (Wiley-Interscience, New York, 1981), p. 77.

12. H.R. Phillip and H. Ehrenreich, Phys. Rev. 129, 1550 (1963).

13. W.H. Latimer, Oxidation Potentials (Prentice-Hall, Englewood Cliffs, 1964).

14. M.J. Madou, K.W. Frese, Jr., and S.R. Morrison, J. Electrochem. Soc. 126, 1827 (1979).

15. M. Cardona, in Semiconductors and Semimetals, Vol. 3, edited by R.K. Willardson and A.C. Beer (Academic, New York 1966), p. 125.

16. E.M. Conwell, Solid State Physics, Supplement 9, edited by F. Seitz, D. Turnbull, and H. Ehrenreich, (Academic, New York, 1967), pp. 155-160.

17. C.V. Shank, R.L. Fork, R.F. Leheny, and Jagdeep Shah, Phys. Rev. Lett. 42, 112 (1979).

18. $\tau_t = \frac{d}{v}$, where $d = 5X10^{-7}$ cm and hole velocity is estimated to be $v = 5 \times 10^6$ cm/s, see e.g.: J.S. Blakemore, J. Appl. Phys. 53, R123 (1982).

Solution	UV-etch rate at 10 W/cm^2 (μm/min)		
	n-type	SI-type	p-type
$H_2SO_4:H_2O_2:H_2O$ :: 1:1:100[a]	18	13	0.8
$HNO_3:H_2O$ :: 1:20[a]	12	10	1.0
$KOH:H_2O$ :: 1:20[b]	8	6	0.5

[a] By volume

[b] By weight

Table I. UV-etch rates for different doping types of GaAs in three etching solutions. The incident laser intensity was 10 W/cm^2.

Figure Captions

Fig. 1 Etch rates for n-type GaAs as a function of laser intensity. Results are compared for green (514 nm) and UV (257 nm) light, and for different solutions:
(a) $H_2SO_4:H_2O_2:H_2O$ = 1:1:100 (by volume),
(b) $HNO_3:H_2O$ = 1:20 (by volume), and
(c) $KOH:H_2O$ = 1:20 (by weight).

Fig. 2 SEM micrographs of a via-hole etched through a 200- μm-thick GaAs sample: (a) via-hole entrance, and (b) cleaved cross section.

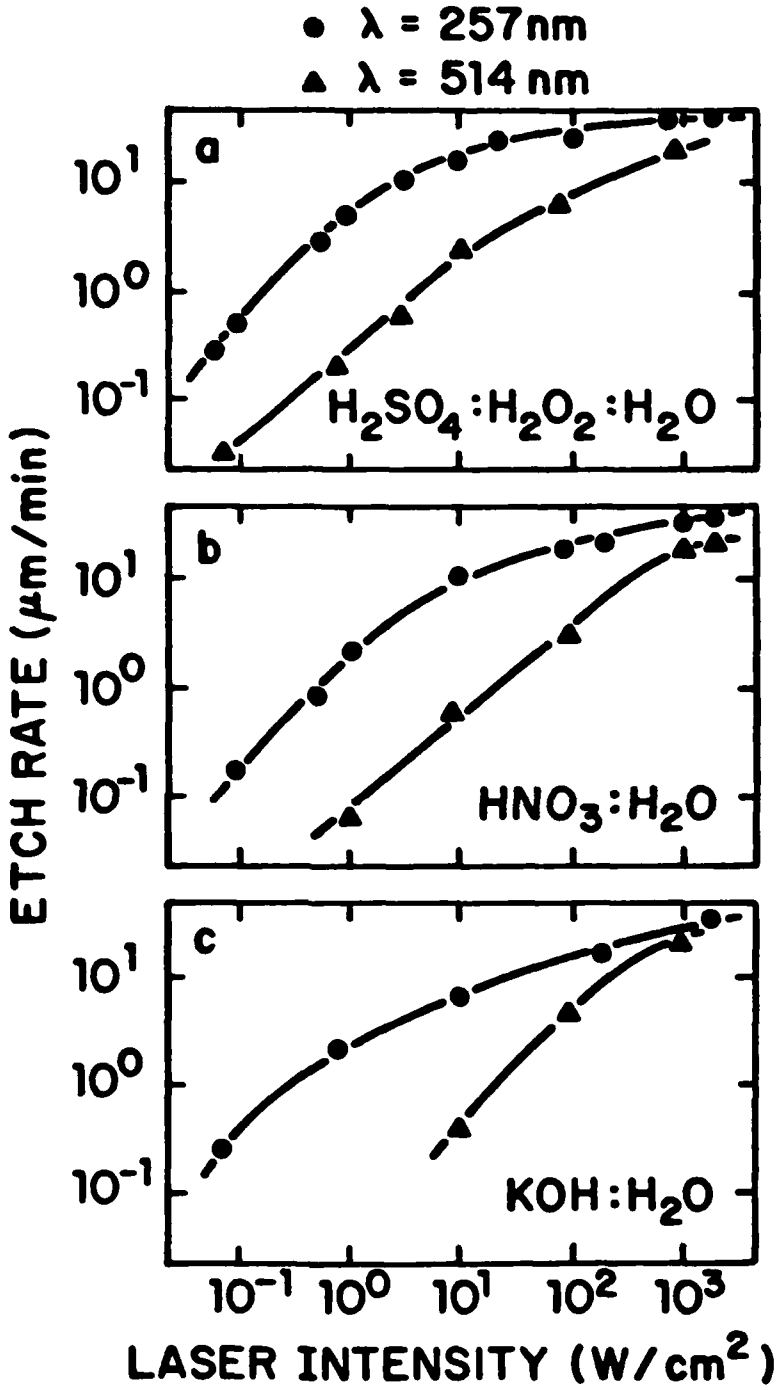
● λ = 257nm
▲ λ = 514 nm
a
b
c
$H_2SO_4:H_2O_2:H_2O$
$HNO_3:H_2O$
$KOH:H_2O$
ETCH RATE (μm/min)
10^1
10^0
10^{-1}
10^{-1} 10^0 10^1 10^2 10^3
LASER INTENSITY (W/cm^2)

Figure 2

a

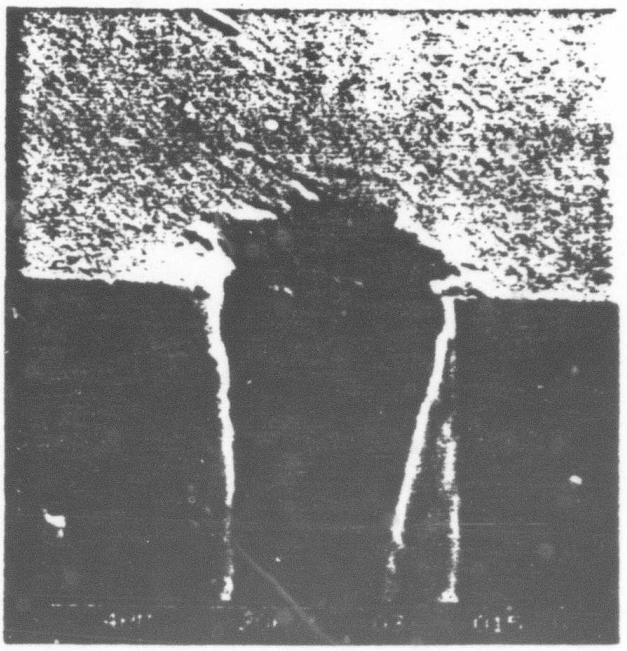

b

Laser-Enhanced Plasma Etching of Si

W. Holber, G. Reksten, and R. M. Osgood, Jr.
Department of Electrical Engineering
Columbia University
New York, New York 10027

Abstract

Laser-enhanced etching of Si in a CF_4/O_2 plasma is described. Both p- and n- type Si were investigated for different dopant concentrations at laser intensities from 0-2 Watts. Etch rate enhancement, due to both thermal and nonthermal effects, were observed and are discussed.

In recent years, laser-controlled, dry-etching processes have been investigated for a wide variety of applications in microfabrication (1,2,3). The use of lasers to influence the etch process offers control of the specific etching chemistry, along with good process anisotropy. In addition, maskless processing, using either a scanned focussed laser beam or a projected imaged beam, has been demonstrated.

Photons in the visible or UV spectral region can enhance the etch rate as a result of a variety of processes, e.g. photodissociative production of gas-phase radicals, surface or gas-phase heating, laser-light-generated photovoltage (in semiconductor substrates), etc. For example, in laser-induced etching of Si in molecular gases such as Cl_2, HCl and XeF_2 (4, 5) thermal and photochemical effects, or a combination of both, were found to be responsible for the etch rates obtained. In addition, in the case of light-induced etching of Si in XeF_2, the etching was in part attributed to the influence of photogenerated charge carriers on the rate of surface reactions.

Plasma etching of Si is a process which has not, to date, been combined with laser etching. In a plasma etcher, generation of the the reactive species occurs by electron-induced dissociation through the glow-discharge. Spatially localized etching requires prior masking of the surface using a contact mask of photoresist, dielectric, or other chemically inert material. Adlayers may be formed on the surface due to reaction products or chamber contaminants; these adlayers inhibit surface etching due to a filling of surface sites and may cause nonuniform etching of the substrate surface. In this paper, we show that laser illumination of the Si surface in a CF_4/O_2 plasma enhances

the plasma etch rate and, further, that the etched area is confined to a region defined by the illuminated area on the surface. The etch enhancement appears to be due to a combination of thermal and nonthermal processes.

In our experiment, a commercial planar plasma etcher was used in conjunction with a cw, argon-ion laser operating on a single line at 514nm. By modifying the radio-frequency (rf) electrode through the installation of an optical port, the laser light could be focussed onto the Si surface with an optical system external to the plasma etcher. The presence of the port did not cause any change in the plasma etch rate. Figure 1 illustrates the experimental arrangement. An 80% CF_4/20% O_2 gas mixture was used, generally at 120 mTorr pressure. The rf power applied to the plasma etcher electrode was typically 0.1 W/cm^2 and the rf frequency 30 kHz.

Fluorine is liberated in the plasma environment typically through the the dissociative ionization reaction:

$$CF_4 + e^- \longrightarrow CF_3^+ + F + 2e^- \qquad (1)$$

Reaction products are adsorbed onto the Si surface and several possible surface reactions lead to the formation of SiF_4, which is volatile. In our system, "dark etch" rates of $\sim$ 0.2 μm/min were typical.

When the laser beam was directed onto the sample both thermal and nonthermal effects were observed. Passing the laser beam above the sample did not cause any effect, indicating that gas phase reactions are unimportant in our experiment. Furthermore, without the plasma discharge, the laser radiation would not etch Si either with or without the CF_4/O_2 ambient.

In an early experiment, an unfocussed laser beam was used, essentially heating the bulk of the Si sample. A second Si sample was placed near the laser-irradiated piece, allowing a comparison between the dark etch rate and the photon-enhanced etch rate to be made. Both Si samples were masked by an aluminum pattern and the etch depth measured with a mechanical stylus. The etch rate of the illuminated sample was significantly enhanced, reaching 2.5 times the dark etch rate at laser powers of 2 W. At this power, the temperature rise of the Si surface was measured to be less than 100°C. When a heat-sink compound was placed between the Si sample and the plasma etcher electrode, the enhancement did not occur, thus indicating that thermal effects were indeed responsible for the increased etch rates.

The local effect of the laser beam on p- and n- type Si of different conductivities (0.006 Ω cm - 52 Ω cm) was investigated by focussing the laser to a 30-100 μm spot on the Si surface. The laser power density varied from 100 W/cm^2 to 124 kW/cm^2. The size of the focussed spot was estimated using the diameter of the etched feature, since the laser beam diameter was difficult to monitor in situ. The diameter of the etched hole was found to stay constant, within experimental error, over the laser-power ranges investigated at each focussing position. Note that in these local-etching experiments, the laser-irradiated piece was thermally contacted by good mechanical clamping to the grounded aluminum cathode. For each measurement made, the dark-etch rate was again monitored by placing a second Si sample near the laser-illuminated piece. The photon-enhanced and the "dark-etch" rates could thus be compared. The enhancement was then normalized against the dark etch rate for each sample of Si investigated.

The results are plotted in Fig. 2. The major source of uncertainty, apart from the above mentioned method of obtaining the beam diameter, was in the measurement of etch depth, which gave rise to an error of ~ 20% in the etch enhancement. The curves show that at high laser powers (>6 kW/cm^2) etching of p- and n- type Si of different conductivities is equally enhanced by the laser, reaching 250% of the dark etch rate at the maximum powers investigated. At these high power densities, a temperature rise in the area of the focal spot is expected. However the good thermal contact between the Si wafer and etcher electrode insured that heating occurred only in the immediate vicinity of the laser spot.

Since our earlier experiments showed that heating of the Si wafer caused significant etch enhancement, calculations were made to estimate the temperature rise at the center of the laser focal spot (7). For a constant laser focal spot and for low laser power densities the temperature will rise linearly with the laser power density; a plot of this variation is shown in the insert to Fig. 3. These calculations include the dependence of the thermal conductivity on temperature and assume total absorbtion of the incident laser light. At 10 kW/cm^2, the calculated temperature rise is 30^{o}C. For this temperature rise the etch rate enhancement, as measured in the unfocussed laser experiment, is not sufficient to ascribe to a purely thermal process. For the higher temperatures (higher intensities) attained in Fig. 2, we believe that, in fact, most of the etch rate enhancement is due to substrate heating in the laser focal region. Since thermal conductivity is largely independent of dopant concentration [8], we expect the curves at high laser powers to be similar for all the doping levels investigated. This does indeed occur at high power densities.

At laser intensities below 1kW/cm^2, however, neither the shape nor the magnitude of the intensity dependent curves, and hence the variation with temperature, are consistent with what would be expected from a simple, thermally enhanced etch rate. In particular, note that for most of the samples studied, the enhancement is substantial even at the lowest laser power investigated. Figure 3 shows this regime by presenting the boxed area in Fig. 2 on an expanded scale. The laser power densities are the same as the range plotted against temperature in the inset in Fig. 3. In this low intensity region, the photon-induced etch enhancement shows a strong doping dependence. The etch enhancement for p- type Si of 1-2Ωcm resistivity (4 x 10^{16}cm^{-3}) is, for example, five times greater than that for p- type Si of 0.0006-0.009 Ωcm (10^{20} cm^{-3}) resistivity at 1 kW/cm^2 incident laser power density.

As mentioned above, one of the advantages of laser-enhancement of the etching process is that it permits localized processing on the wafer surface. Although our optical set-up did not permit high-resolution studies to be made, we were able to use the present experimental arrangement to obtain a minimum diameter of 30 μm for the etched hole. Interference fringes of 10 μm dimension were, however, visible in the etched pattern, indicating that laser-enhanced plasma etching allows high-resolution control of spatial features. In a reactor properly shielded from vibrations, higher pattern definition can be expected.

A number of surface reaction steps lead to the etching of Si in the CF_4/O_2 plasma, and many of these might be enhanced directly by photons, or by a photon-induced temperature rise. While it is not possible to

identify precisely which steps are responsible for the laser enhancement of the etch rate from the experiments described here, some general comments can, however, be made about the various etching processes.

In particular, as shown in Fig. 2, the etch enhancement appears to saturate at high laser intensities. This behavior is consistent with a simple first-order reaction scheme which is, for example, transport limited at high temperatures. Similarly, the low intensity, or nonthermal enhancement seen for all except the heavily p-doped material also appears to exhibit a saturation phenomena. This is again consistent with a first-order reaction process, in which at least one step is not dependent on the light intensity, and thus becomes rate-limiting.

A recent study regarding the specific mechanism of nonthermally enhanced laser-assisted etching of Si by XeF_2, with no plasma discharge, showed that light can enhance the reaction rate between fluorosilicon groups and adsorbed fluorine on the surface, thus increasing the overall etch rate. (9, 10) This increased reaction rate was attributed to the flow of photogenerated minority carriers to surface sites. In the case of p-type Si, electrons combine with adsorbed fluorine at the surface. For n-type Si, holes combine with SiF_x sites at the surface. In both cases, the resultant Coulombic force between reactants yields a higher reaction cross-section.

The doping dependence we observed at low laser power densities indicate that the process responsible for the nonthermal enhancement is in our case also related to charge carriers on the surface. The fact that both p-and n- type Si exhibit photon enhanced etch rates is consistent with the above mentioned theory since positive or negative

photogenerated minority carriers, respectively, give rise to enhanced surface reaction rates.

Another possible mechanism by which the laser can enhance the silicon etch rate is through desorption of polymer layers which can form on the silicon surface. Polymer layers can inhibit the etch process through two mechanisms -- either by blocking surface reaction sites, or by consuming fluorine[11, 12]. Both thermal and non-thermal effects from the laser could increase the desorption rate of these polymers. It is not clear, however, whether this model for the photon-enhanced-etching process would include an explanation for the observed doping dependence at low laser power densities.

In conclusion, we have shown that etching of Si in a CF_4/O_2 plasma is significantly enhanced by illumination with a visible cw laser. The enhancement consists of a thermal and a nonthermal component. In the nonthermal regime the enhancement is strongly dependent on doping concentration, and is substantial for both p- and n- type Si. The applications of laser-enhanced plasma etching range from direct writing of local etching patterns to controlling the process rate and spatial features in a plasma reactor.

We thank Drs. Heinz Gilgen and Peter Brewer for many helpful discussions. This work was sponsored by the Defense Advanced Research Project Agency, the Air Force Office of Scientific Research, and the Joint Services Electronics Program.

References

1. D.J. Ehrlich, R.M. Osgood, Jr. and T.F. Deutsch, IEEE J. Quantum Electron. QE-16, 1233 (1980).
2. T.J. Chuang, J. Chem Phys. 74, 1461 (1981); J. Vac. Sci. Technol. 18, 638 (1981); J. Vac. Sci. Technol. 21, 798 (1982).
3. D.J. Ehrlich and J.Y. Tsao, J. Vac. Sci. Technol. B, 4, 969 (1983).
4. D.J. Ehrlich, R.M. Osgood, and T.F. Deutsch, Appl. Phys. Lett. 38, 1018.
5. F.A. Houle, Chem. Phys. Lett. 95, 5 (1983).
6. T.J. Chuang, J. Chem. Phys. 74, 1453 (1981).
7. M. Lax, J. Appl. Phys. 48, 3919 (1977); M. Lax, Appl. Phys. Lett. 33, 786 (1978).
8. S.M. Sze, Physics of Semiconductor Devices, Wiley, New York (1981).
9. F.A. Houle, J. Chem. Phys. 79, 4237 (1983).
10. F.A. Houle, J. Chem. Phys. 10, 4851 (1984).
11. D.L. Flamm, V.M. Donnelly, D.E. Ibbotson, J. Vac. Sci. Technol. B, 1, 23 (1983).
12. J.W. Coburn and H.F. Winters, J. Vac. Sci. Technol., 16, 391 (1979).

Figure Captions

Fig. 1 Experimental arrangement for demonstrating laser-assisted etching of silicon.

Fig. 2 Laser-induced etch enhancement versus laser power density for different dopant concentrations.

Fig. 3 Laser-induced etch enhancement versus laser power density, boxed area in Fig. 2. The inset shows the calculated laser-induced temperature rise versus laser power density for a 95 μm diameter focal-spot size.

MASKLESS LASER WRITING OF SILICON DIOXIDE

R.R. Krchnavek, H.H. Gilgen, R. M. Osgood, Jr.

Department of Electrical Engineering
Columbia University
New York, NY 10027

ABSTRACT

A laser direct writing technique for forming insulating layers of silicon dioxide from an organosilicate film on various substrate materials is shown. The process resolution is a function of the thermal properties of the substrate and is shown to be 1 μm. The technique allows for a local variation in the oxide thickness by changing process parameters. The quality of the laser written layers is compared to similar films formed by conventional organosilicate processing.

Maskless Laser Writing of Silicon Dioxide

I. INTRODUCTION

As integrated circuits become more complex, the need for maskless techniques of metallization, doping, and insulator formation become important in the areas of repair and customization. In this letter, we describe a maskless technique for patterning silicon dioxide layers. Using spin-on organosilicates, a focused laser beam is used to directly write silicon dioxide patterns on a variety of substrates. The quality of the oxide layers is at least as good as that obtained in thermally cured spin-on glass. An added advantage of this technique is the ability to readily vary the thickness of the oxide layer as a function of the position on the substrate. Some possible applications include local masking for GaAs, SiO_2 waveguides for silicon wafers and new device structures requiring a variable oxide thickness.

II. EXPERIMENTAL

The writing of oxide layers is accomplished using the experimental setup shown in Figure 1. The Argon ion laser is tuned to 514.5 nm and a microscope objective (20X, N.A.=0.35) coupled with a Michelson interferometer is used to focus the laser beam onto the sample. The sample is mounted on a vacuum chuck which is attached to a computer-controlled, X-Y translation stage. The stage is driven by a stepper motor with 0.4 μm resolution and linear scanning rates from 4μm/sec to 200 μm/sec. Blanking of the laser beam is accomplished with a computer-controlled mechanical shutter. The starting material, an experimental material provided by Allied Corporation known as X-200A, is an organosilicate material in an organic based solvent with the general formula

of $Si(OR)_x(OH)_{4-x}$. During thermal curing, it initially undergoes an elimination reaction expelling the organic liquid. At higher temperatures, the OH groups are driven off leaving a layer of SiO_2.[1] Wafer preparation consists of washing with a cleaning solution such as hot H_2O_2:H_2SO_4 followed by an H_2O:HF rinse with subsequent application of the organosilicate via spinning. The sample is spun at 3000 RPM for 30 seconds to produce a glass-like film. Deposited film thickness is both a function of the spin speed and the viscosity of the organosilicate solution. Typical deposited films in this work are approximately 5000-Å thick. Thinner films can be achieved by reducing the viscosity of the organosilicate by addition of the proper solvent while thicker films can be produced by reducing the spinner rotational speed.

Writing was attempted over a wide range of scan speeds, focal-spot sizes and laser powers. Typical conditions were 250 mW in a 3 μm diameter spot which corresponds to 4 MW/cm^2 and a sample translation speed of 100 μm/sec. With these experimental parameters, a smooth, continuous line could be obtained. To remove the unexposed material, it is necessary to rinse the wafer with methanol. The cured pattern then remains. In order to obtain a complete removal of the unexposed material, it is necessary to carefully preclean the wafers and to keep the samples under conditions of low relative humidity. At temperatures near 400° C, X-200A is very hygroscopic and should therefore be used when the ambient relative humidity at 20° C is less than 50%. An alternate technique for removing the unexposed material is to use a rinse of very diluted HF. In contrast to the methanol rinse, however, this solution will remove both exposed and unexposed material with the exposed material being removed at a slower rate. This approach was not used in the experiments reported here.

III. RESULTS AND DISCUSSION

Figure 2a shows a scanning electron microscope (SEM) micrograph of a part of a silicon dioxide line pattern on a silicon substrate. Its 3.5 μm width is determined by the optical spot size and the temperature distribution on the surface; smaller line widths could be obtained by the use of a higher magnification objective. To obtain the high quality corners seen in Figure 2a, one must momentarily block the incident laser beam to prevent undesired heat spreading while the translation stage changes direction. Using a 50X microscope objective, the line shown in Figure 2c was obtained. The structure on the outer edges of the line demonstrates the non-linear nature of the curing process. Subsequent rising in a very diluted HF solution as described earlier will remove this structure producing a line on the order of 1 μm. The mechanical integrity of these lines appears good with no visible signs of stress cracking; the lines hold up well against a cellophane-tape pull. Quantitative adhesion and stress tests have not been performed. The dielectric breakdown strength of the laser formed oxide layers was obtained by scanning the beam to produce an oxide layer large enough for probing. The breakdown strength was measured at 1.6×10^6 V/cm. This compares favorably with thermally cured oxide layers at 10^6 V/cm and thermally grown silicon dioxide at 10^7 V/cm.

Curing of organosilicate films by laser-induced heating is significantly different from conventional thermal curing in a furnace. Furnace curing requires that either the temperature be slowly ramped or a low-temperature cure (100° C) precedes the final high temperature cure. Curing of the organosilicate occurs from the outer surfaces of the film toward the center. As the organosilicate cures in the furnace, the volatile components must pass through the cured outer regions. If the sample temperature is not ramped in the furnace or preceeded by a low temperature cure, surface cracks resulting

from the escaping volatile components can result. In laser curing, on the other hand, since the organosilicate is essentially transparent in the visible region, the laser beam passes through the film and strikes the surface of the silicon substrate where it is partially absorbed thereby heating it up. Curing of the organosilicate film occurs from the organosilicate-substrate interface outward allowing volatile components to escape easily, since the surface of the layer had not been cured first. This allows for high substrate surface temperatures during curing without cracking the organosilicate layer.

A further result of the organosilicate curing from the organosilicate-substrate interface outward is that if the exposure time is insufficient to cure the entire thickness of the deposited organosilicate, a cured organosilicate layer thinner than the deposited layer can be obtained. This gives a thickness, or z-axis control over the oxide layer. This smooth control over the thickness of local regions of oxide is not easily achieved through conventional photolithography. In addition to the thickness variation, the width of the oxide lines is also a function of the translation speed and incident power. Figure 2d shows the effect on line width as the incident power is ramped up and down while maintaining a constant translation speed. A graph of the experimental results showing both the oxide thickness and oxide width as a function of scan speed and incident power is depicted in Figure 3. Of particular interest is the oxide thickness obtained with 0.32 Watts which is constant over the range of scan speeds tested indicating the entire spin-on layer has been cured. For laser powers below 0.32 Watts or for faster scan rates, the irradiation time is only sufficient to cure a portion of the layer next to the substrate. Note that for all power levels, however, a variation in the scan speed results in a change of the line width. Furthermore, the line width varies nonlinearly between 0.25 Watts and 0.32 Watts.

The curing of the organosilicate layer is a complex phenomena which involves both the evaporation of the volatile species followed by diffusion through the layer and the various chemical reactions between the constituents of the film. These factors cause a temperature and curing gradient to be established within the organosilicate layer which determines the variation in linewidth and film thickness with laser power. Both of these phenomena depend on the temperature of the organosilicate layer. The temperature of the organosilicate layer is a function of the heat flow into the layer with the surface of the substrate acting as the heat source. For the spin-on layer, the temperature distribution on the surface of the substrate can be approximated by solving the heat equation for a focused Gaussian beam on a bare silicon substrate[2]. Furthermore, although the beam is being scanned, the scanning speeds are slow enough to assume the substrate temperature distribution within the beam is given by the steady-state temperature distribution.[3,4] At 0.32 Watts of incident laser power, the maximum calculated temperature is approximately 370°C.

By considering a simple one-dimensional treatment of the evaporation front which moves out from the silicon wafer, it is possible to show that evaporation is not the rate limiting process.[5] The curing rates in our work are more in agreement with an elimination reaction with an activation temperature, E_a/k, above the temperature attained in these experiments, where E_a is the chemical activation energy and k is Boltzmann's constant. To determine the width and thickness of a cured line for a given laser power level and sample scanning speed requires accurate knowledge of the temperature distribution within the organosilicate layer. However, the temperature distribution in the organosilicate layer is a complex function affected by the heat flow within the layer, the energy dissipated during solvent evaporation, and the energy dissipated during the reaction. Further complications occur

when the entire thickness of the organosilicate layer has been cured because heat is no longer consumed in reacting the organosilicate in the thickness direction and the heat flow is directed outwards thereby increasing the line width. These affects, in addition to the change in film optical properties with curing thickness, may account for the nonlinearity in linewidth variation in going from 0.25 Watts to 0.32 Watts as shown in Figure 3.

Because of the organic nature of the material, the C and H content of the film and hence the degree of curing of the laser-formed layers was determined by comparing their infrared (IR) spectra with those of thermally cured layers.[1] Figure 4 shows IR absorption spectra for four different samples: spin-on only, low-temperature cure at 100° C for 10 minutes, low-temperature cure plus an additional one hour cure at 800°C and a laser-formed oxide. The principal bands of interest occur in the 1100 cm^{-1} region including the Si-O stretch at 1075 cm^{-1} and the Si-O-C stretch from 1100 to 1000 cm^{-1}. As the organosilicate is heated, it decomposes producing volatile components and leaving a predominantly SiO_2 film. This is shown in Figure 4 by the decrease in the Si-O-C band and a corresponding sharpening of the Si-O band in going from the spin-on sample to the high-temperature cured sample.

The hydroxyl group, which is present in both the silicate and the alcohol solvent, has a broad stretching vibrational band at approximately 3300 cm^{-1}. This band is seen in all of the spectra although it is weakest in the high temperature cured sample. In addition to the O-H stretch, the bending vibration for Si-O-H at 870-820 cm^{-1} appears in the spun-on and the low-temperature cured samples but is virtually gone in the high-temperature cured sample.

The symmetric and asymmetric stretching vibration of the C-H group and the bending vibrations of the CH_3 group produce peaks near 3000 and 1400 cm^{-1} respectively. These C-H bands are due primarily to the solvent and are easily

removed after the initial heating as can be seen in the spectra of the low-temperature cured sample.

Comparing the IR spectra of the thermally cured samples with the laser-cured sample, we see that the laser-formed oxide layer is similar to samples that have undergone a low-temperature cure and, therefore, has significant quantities of Si-O-C and Si-O-H remaining. These can be removed by further heating with no noticeable cracking or loss of adhesion.

We have experimented with substrate materials other than silicon. These include the compound semiconductors CdS and GaAs and the dielectric SiO_2. In each case, after a proper surface preparation and adjustment of incident laser power to account for different absorption and thermal properties, direct writing of oxide lines was readily accomplished. In particular for GaAs, surface preparation consisted of a standard degreasing and oxide removing cleaning procedure. Consistent with the thermal and absorption properties of GaAs, direct writing was done at 0.1 Watts for scan speeds similar to those used above.

IV. CONCLUSIONS

In conclusion, we have demonstrated a method of patterning silicon dioxide layers on various substrate materials without the use of a mask. The technique relies upon the curing of a spin-on organosilicate by localized heating with a focused laser beam. Translation of the sample provides for maskless pattern generation. Line widths as low as 1 μm have been obtained. Both line width and line thickness are affected by the sample translation speed and the incident laser power. This means that silicon dioxide lines of continuously varying thickness can be written on the wafer surface. This cannot be easily achieved through conventional photoresist techniques and lends itself to the fabrication of unique microstructures. The quality of the

deposited layers is at least as good as spin-on organosilicate layers cured at low temperature, thus making these patterns suitable for use as masking material and waveguide structures. Furthermore, high-temperature curing after patterning may also produce higher quality silicon dioxide layers for interlayer dielectrics.

ACKNOWLEDGEMENTS

We thank James Yardley and Steve Kirtley for supplying materials and for many helpful discussions. This work was supported by the Defense Advanced Research Project Agency, the Air Force Office of Scientific Research, and the National Science Foundation.

REFERENCES

1. S. Kirtley, (private communication).

2. M. Lax, in Laser-Solid Interactions and Laser Processing, edited by S.D. Ferris, H. J. Leamy, and J. M. Poate (American Institute of Physics, New York, 1978), p.149.

3. J. E. Moody and R. H. Hendel, J. Appl. Phys., 53, 4371 (1982).

4. Y. I. Nissim, A. Lietoila, R. B. Gold, and J. F. Gibbons, J. Appl. Phys., 51, 274 (1980).

5. R.M. Osgood, Jr., H.H. Gilgen, R.R. Krchnavek, (unpublished work).

FIGURE CAPTIONS

Fig. 1. Schematic diagram of the maskless laser-writing system.

Fig. 2. SEM micrograph of a typical silicon dioxide line on a silicon substrate. Incident laser intensity was 4 MW/cm^2 with a scanning speed of 100 μm/sec (typical).
(a) Top view.
(b) Cross section on a cleaved substrate.
(c) 1 μm wide silicon dioxide line produced at 4 MW/cm^2 using a 50X microscope objective.
(d) Variation in silicon dioxide line width as the incident laser power is ramped up and down.

Fig. 3. (a) Silicon dioxide thickness versus scanning speed for various incident laser power levels and a 3 μm spot size.
(b) Silicon dioxide line width versus scanning speed for various incident laser power levels and a 3 μm spot size.

Fig. 4. Infrared absorption spectra of four different organosilicate layers: (a) as deposited, (b) after a low-temperature cure, (c) after a high-temperature cure, (d) typical laser formed.

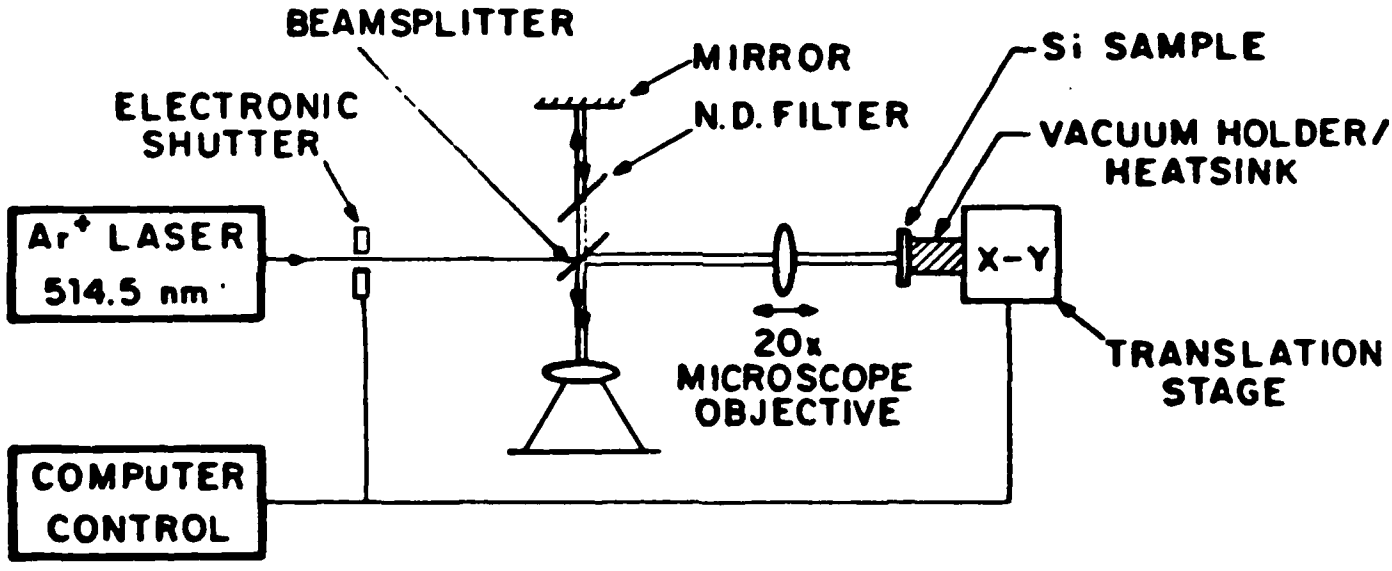
BEAMSPLITTER
MIRROR
Si SAMPLE
ELECTRONIC SHUTTER
N.D. FILTER
VACUUM HOLDER/ HEATSINK
Ar+ LASER 514.5 nm
X-Y
20x MICROSCOPE OBJECTIVE
TRANSLATION STAGE
COMPUTER CONTROL

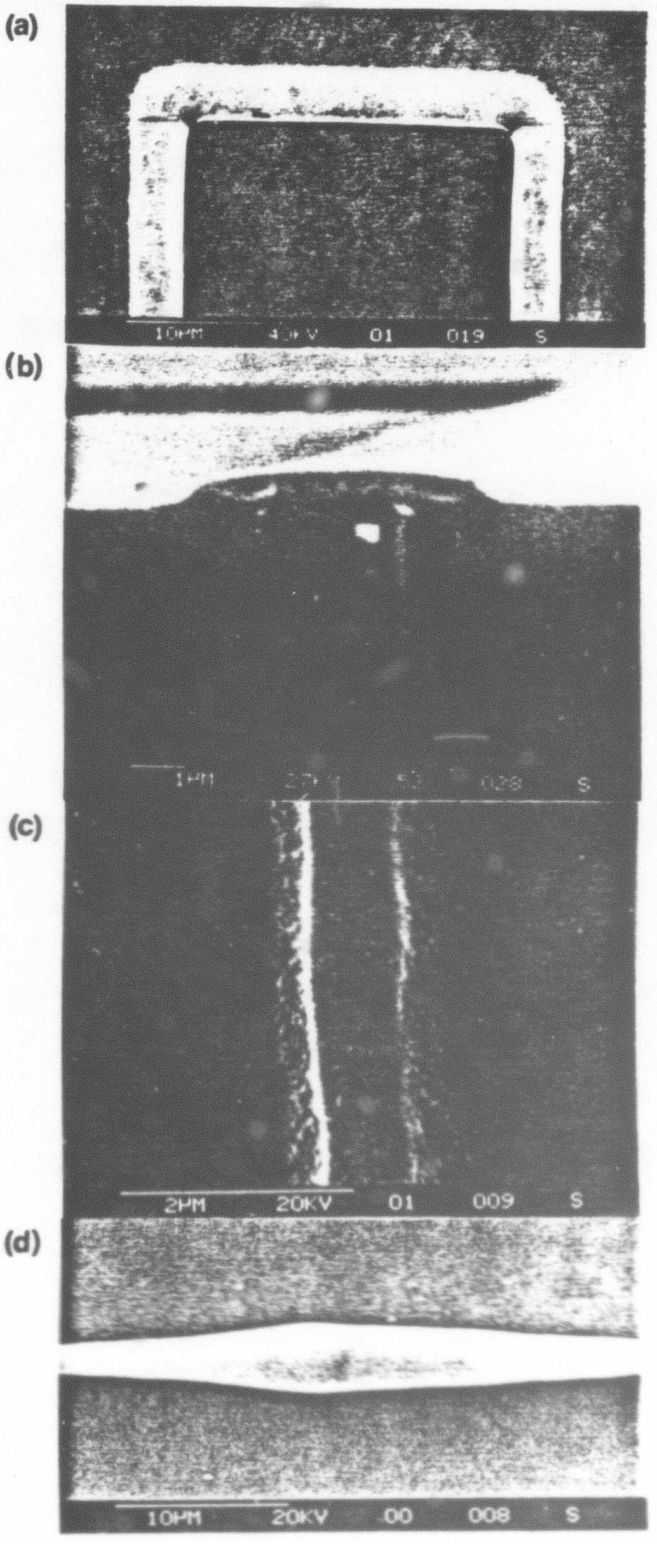
(a)
10PM 4.0KV 01 019 S
(b)
1PM 20KV 01 028 S
(c)
2PM 20KV 01 009 S
(d)
10PM 20KV 00 008 S

(a) OXIDE THICKNESS vs SCAN SPEED FOR VARIOUS POWER LEVELS

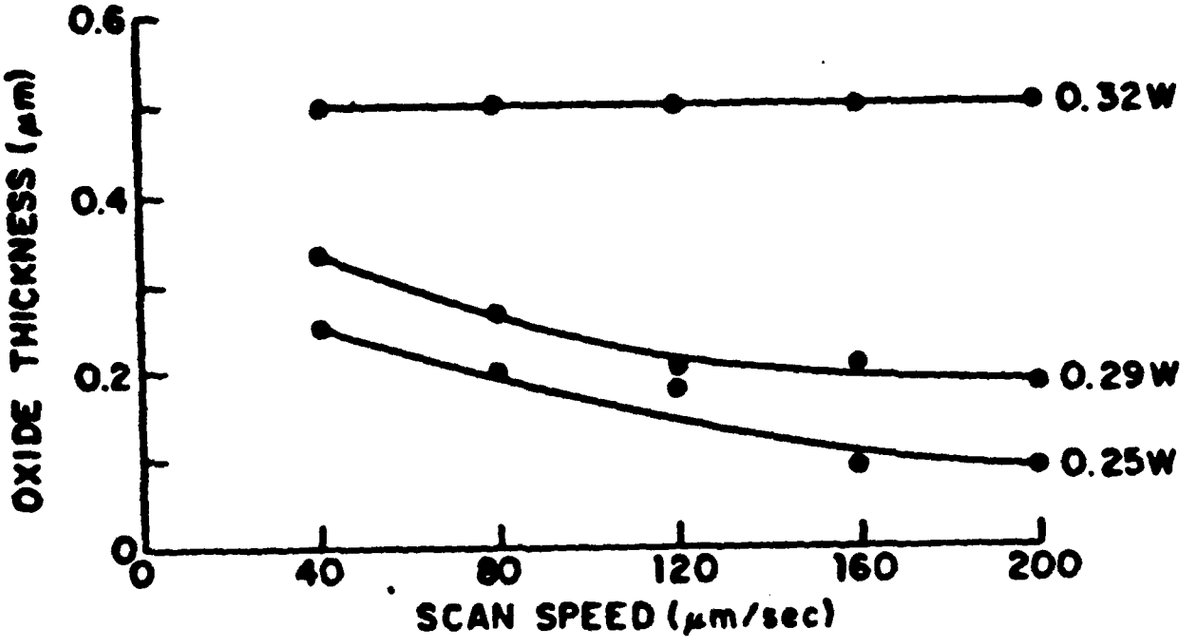

(b) OXIDE WIDTH vs SCAN SPEED FOR VARIOUS POWER LEVELS

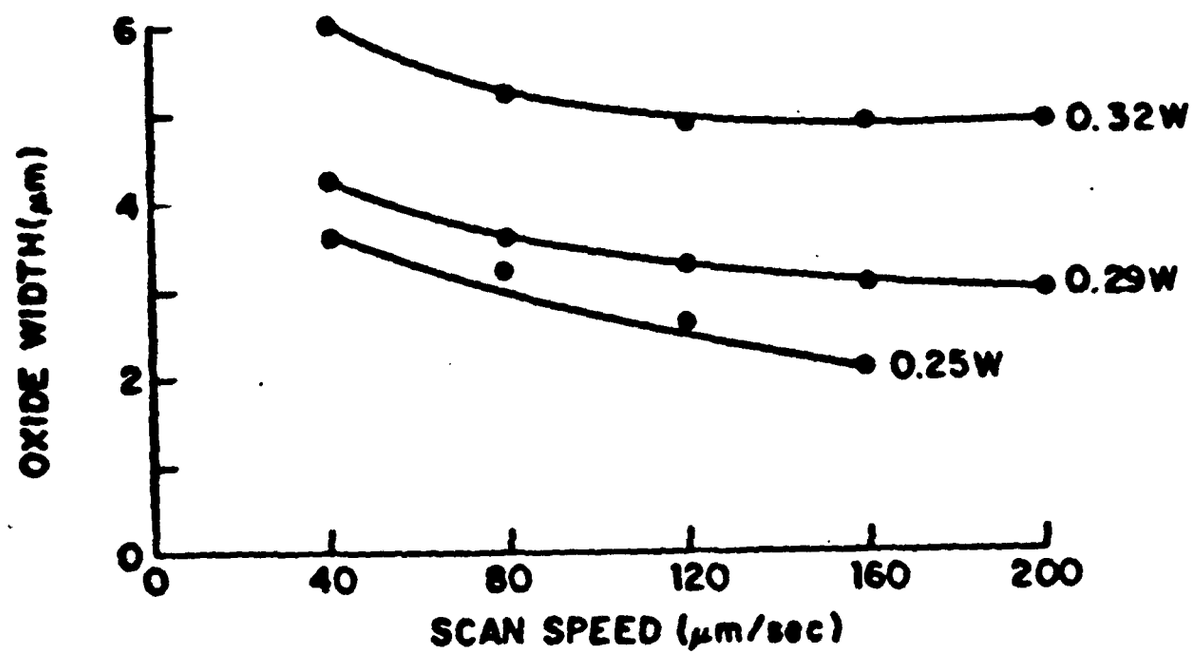

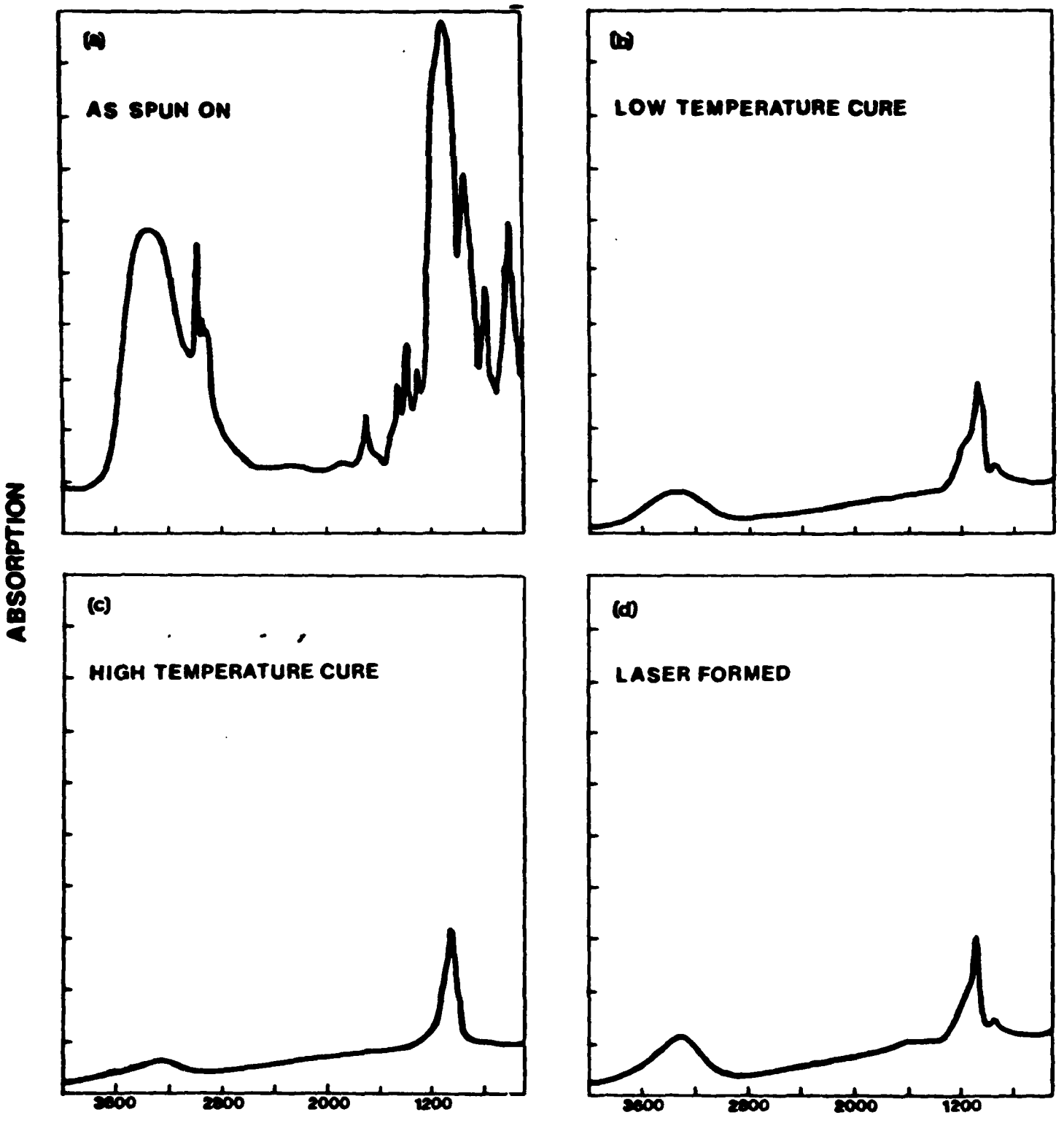
(a)
AS SPUN ON
(b)
LOW TEMPERATURE CURE
(c)
HIGH TEMPERATURE CURE
(d)
LASER FORMED
ABSORPTION
3600
2800
2000
1200
3600
2800
2000
1200
WAVENUMBERS (cm-1)